mater.scichina.com link.springer.com

Published online 23 January 2024 | https://doi.org/10.1007/s40843-023-2754-8
Sci China Mater 2024, 67(2): 424–443

SPECIAL TOPIC: Heterojunction in Photocatalysts

TiO_2-based S-scheme photocatalysts for solar energy conversion and environmental remediation

Baolong Zhang, Bin Sun*, Fangxuan Liu, Tingting Gao and Guowei Zhou*

ABSTRACT **Solar-driven semiconductor photocatalysis technology is deemed to be a potential strategy to alleviate environmental crisis and energy shortage. Thus, the exploration of high-efficiency photocatalysts is the key to promoting the development and practical application of photocatalysis technology. As a typical photocatalyst, TiO_2 has gained extensive attention because of its superb stability, environmental-friendliness, and low price. However, the rapid photo-induced carrier recombination, inadequate light absorption, and insufficient reduction capacity are still the major drawbacks that significantly hamper its photocatalytic performance. Fortunately, the above shortcomings can concurrently overcome by constructing TiO_2-based step-scheme (S-scheme) heterojunction photocatalysts with other semiconductors, during which the respective advantages can not only achieve significant spatial carrier separation and robust light-harvesting ability but also preserve the strong redox capacities. Herein, this review presents the latest development in improving the photocatalytic performance of TiO_2 *via* the S-scheme heterojunction. Specifically, the classification of TiO_2-based S-scheme heterojunction photocatalysts has been detailly described, mainly including metal oxides, metal chalcogenides, organic semiconductors, and other semiconductors. Then, we summarize the current research progress of TiO_2-based S-scheme heterojunction photocatalysts in photocatalytic H_2 evolution, CO_2 reduction, H_2O_2 production, and pollutant degradation. Simultaneously, various characterization strategies for understanding the photo-induced carrier transfer pathway are also reviewed. Finally, we propose several drawbacks and future prospects in the development of TiO_2-based S-scheme heterojunction photocatalysts. It presents an insight into constructing high-efficiency TiO_2-based S-scheme heterojunction photocatalysts for energy conversion and environmental remediation.**

Keywords: TiO_2, step-scheme heterojunction, photocatalysis, energy conversion, environmental remediation

INTRODUCTION

With the development of modern industry and economy, the energy shortage and environmental crisis are urgent to solve the major issues that restrict the long-term development of mankind society. Photocatalysis technology, as a clean and continuable strategy, is widely followed in addressing current problems through solar-driven semiconductors [1–3]. Thus, the exploration of efficient semiconductor photocatalysts is of great significance to boost the development of photocatalysis technology. To date, various photocatalysts, such as metal oxides (TiO_2, ZnO, and SnO_2), metal chalcogenides (CdS, $MoSe_2$, and $ZnIn_2S_4$), and organic semiconductors (g-C_3N_4, perylene diimide, and covalent organic frameworks (COFs)) [4–6], have been extensively employed for photocatalysis. Among these studied photocatalysts, TiO_2, as a well-known metal oxide, has sparked extensive research since it served as the photoelectrode material for water splitting [7]. Henceforward, many efforts have been made in the design and controllable preparation of high-efficiency TiO_2 photocatalysts. However, a single TiO_2 photocatalyst exhibits an inferior photocatalytic performance in most cases, resulting from the high photo-induced carrier recombination rate, inadequate light absorption, and insufficient reduction ability [8–11]. Hence, more efficient strategies should be explored to boost the photocatalytic performance of TiO_2.

Nowadays, numerous strategies have been developed to overcome the above drawbacks, including morphology modulation, metal and nonmetal doping, crystal surface engineering, co-catalyst deposition, and heterojunction construction [12–17]. As for the aforementioned modification strategies towards TiO_2, constructing a heterojunction is regarded to be one of the particularly effective approaches to further enhance photocatalytic performance. Based on its charge transfer mechanism, TiO_2-based heterojunction photocatalysts are mainly divided into type-II, Z-scheme, and step-scheme (S-scheme) heterojunctions [18–20]. In the type-II heterojunction system (Fig. 1a), the photo-induced electrons can be transferred from photocatalyst I (PCI) to photocatalyst Ⅱ (PCII), while the photo-induced holes migrate in reverse. Despite the fact that type-II heterojunction appears to facilitate photo-induced carrier separation in space, it still has some shortcomings through careful observation. The photo-induced electrons concentrate on the conduction band (CB) of PCII with weak reduction potential and holes concentrate on the valence band (VB) of PCI with weak oxidation potential, leading to a decrease in redox capacity of photocatalytic reaction [21–23]. Simultaneously, the partial energy is also wasted and fails to promote the photocatalytic reaction [23]. Besides, the repulsion from similar charges also restrains the

Key Laboratory of Fine Chemicals in Universities of Shandong, Jinan Engineering Laboratory for Multi-scale Functional Materials, School of Chemistry and Chemical Engineering, Qilu University of Technology (Shandong Academy of Sciences), Jinan 250353, China
* Corresponding authors (emails: binsun@qlu.edu.cn (Sun B); gwzhou@qlu.edu.cn (Zhou G))

continuous migration [24]. Thus, the type-II heterojunction is controversial in terms of thermodynamics, dynamics, and energy. To solve the deficiency of type-II heterojunctions, a traditional Z-scheme heterojunction system is proposed for improving the photo-induced carrier separation and preserving a superior redox capacity [25,26]. As shown in Fig. 1b, c, the photo-induced electrons in the CB of PC Ⅱ are quenched from holes in the VB of PC Ⅰ by a shuttle redox ion-pairs (D and A) or metal conductor. However, in fact, the photo-induced carrier with strong redox capacity is inclined to integrate with shuttle redox ion-pairs in the liquid-phase Z-scheme heterojunction and metal conductor in the all-solid-state Z-scheme heterojunction, respectively [23,27,28].

To eliminate the irrationality of the photo-induced carrier transfer route in the above two types of heterojunction systems, Yu and co-workers [29] innovatively reported an S-scheme heterojunction in 2019, which systematically explained the carrier transfer mechanism in photocatalytic reaction. Since then, the S-scheme heterojunction photocatalysts have experienced a period of significant growth and progress [30–33]. Up to now, numerous researchers have summarized the construction of S-scheme heterojunctions from different perspectives, such as ZnO, g-C_3N_4, and $ZnIn_2S_4$, based S-scheme heterojunction photocatalysts [28,34,35]. Notably, it significantly improved photocatalytic performance in the S-scheme heterojunction system. Generally, an S-scheme heterojunction contains two different types of photocatalysts with staggered band alignment, namely oxidative photocatalyst (OP) and reductive photocatalyst (RP), as illustrated in Fig. 1d. The RP shows more negative CB potential, VB potential, and Fermi level in comparison with OP. Because of its different Fermi levels, the electrons in the RP can migrate to OP after intimate contact between them, forming the internal electric field in the direction of RP to OP. Simultaneously, the energy bands of RP and OP will also bend upward and downward at the interface until the Fermi levels are matched, respectively [23,24]. With light irradiation, the photo-induced electrons on the CB of OP with weak reduction potential are instantly quenched by holes on the VB of RP with weak oxidation potential, which should be associated with the energy band bending, internal electric field, and Coulombic attraction [36–38]. Hence, the S-scheme heterojunction not simply facilitates photo-induced carrier separation and transfer, but additionally retains the strong redox capacity.

Although numerous studies have been reported on TiO_2-based S-scheme heterojunction photocatalysts for photocatalytic applications, there have been few comprehensive reviews to summarize the classification of TiO_2-based S-scheme heterojunction photocatalysts with other semiconductors. Herein, we provide a concise design principle and a comprehensive classification of TiO_2-based S-scheme heterojunction photocatalysts, e.g., metal oxides, metal chalcogenides, organic semiconductors, and other semiconductors. Furthermore, the applications of TiO_2-based S-scheme heterojunction photocatalysts for photocatalytic H_2 evolution, CO_2 reduction, H_2O_2 production, and pollutant degradation are outlined in detail (Fig. 2). Meanwhile, some effective characterization methods are employed to demonstrate the photo-induced carrier transfer pathway and formation of S-scheme heterojunction. Finally, some shortages and future direction of TiO_2-based S-scheme heterojunction photocatalysts are analyzed through the current research progress.

DESIGN PRINCIPLE AND CLASSIFICATION OF TIO_2-BASED S-SCHEME HETEROJUNCTION PHOTOCATALYSTS

Design principle of TiO_2-based S-scheme heterojunction photocatalysts

Generally speaking, the energy band structure of photocatalysts is the key to designing the S-scheme heterojunction [39,40]. As a typical photocatalyst, the Ti 3d orbitals in the TiO_2 construct the CB bottom, while the VB top is mainly determined by the O 2p orbitals, generating a wide bandgap of about 3.2 eV [41,42]. Due to a more positive potential of VB (approximately +2.6 eV),

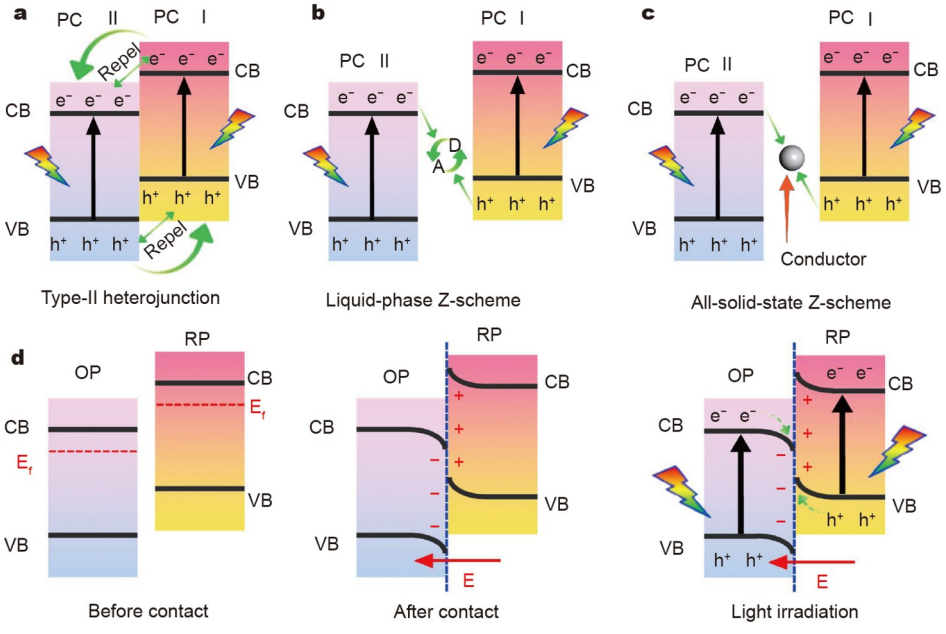

Figure 1 Charge-transfer pathways for (a) type-II, (b) liquid-phase Z-scheme, (c) all-solid-state Z-scheme, and (d) S-scheme heterojunction photocatalytic systems. The labels D and A denote the electron donor and acceptor in (b), respectively.

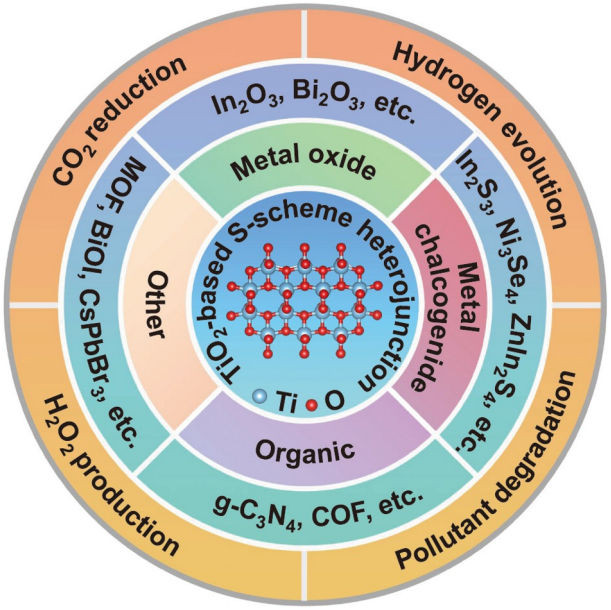

Figure 2 Controllable preparation and application of TiO_2-based S-scheme heterojunction photocatalysts.

TiO_2 can usually serve as an ideal oxidation photocatalyst [41,43]. According to the design principle of S-scheme heterojunction, TiO_2 will integrate with the reduction semiconductor to construct TiO_2-based S-scheme heterojunction photocatalysts, e.g., metal oxides (Bi_2O_3, In_2O_3) [44,45], metal chalcogenides (In_2S_3, Ni_3Se_4, $ZnIn_2S_4$) [46–48], organic semiconductors (g-C_3N_4, COF) [49,50], and other semiconductors (metal-organic framework (MOF), $CsPbBr_3$) [51–53]. In addition to introducing the classification of TiO_2-based S-scheme heterojunction photocatalysts, we also introduce the preparation methods in the following content, such as hydrothermal [54], solvothermal [55], low-temperature reflux [56], physical mixing [57], and other methods [12,58]. Furthermore, the dimensionality of photocatalysts also plays a crucial role in the construction of S-scheme heterojunctions to boost photocatalysis [59–61]. It is possible to synergize and superimpose the advantages of various dimensional photocatalysts by constructing S-scheme heterojunctions, which can provide more active sites, higher light-harvesting ability, and faster photo-induced carrier transfer efficiency [22,62,63]. These contents will also be elaborated in the following work to construct the TiO_2-based S-scheme heterojunction photocatalysts.

Classification of TiO_2-based S-scheme heterojunction photocatalysts

TiO_2/metal oxide S-scheme heterojunction photocatalysts

Due to the excellent chemical stability, controllable morphology, environmental friendliness, and low cost, metal oxide nanomaterials are considered to be potential photocatalysts [64–66]. Thus, by selecting a suitable band structure of metal oxide semiconductors for constructing TiO_2-based S-scheme heterojunction photocatalysts, the superior photocatalytic performance will be well obtained.

For example, He *et al.* [44] constructed a floatable polystyrene (PS) spheres supported TiO_2/Bi_2O_3 S-scheme heterojunction photocatalyst by hydrothermal and photodeposition methods (Fig. 3a). As displayed in Fig. 3b, the shell thickness of S-scheme heterojunction photocatalyst is about 25 nm. Due to its unique floatability (Fig. 3c), the floatable photocatalyst significantly enhances light-harvesting ability and elevates the intimate contact with reactants, which is good for improving photocatalytic performance. In addition to being served as a reduction photocatalyst, Bi_2O_3 can also be used as an oxidation photocatalyst.

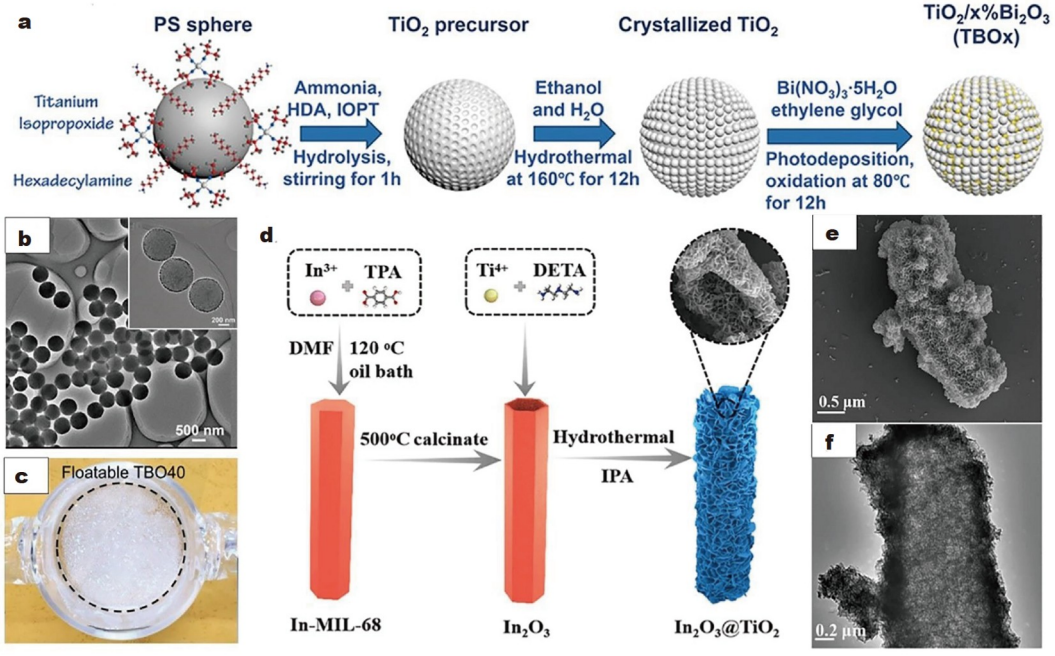

Figure 3 (a) Synthesis process of Bi_2O_3/TiO_2 S-scheme heterojunction photocatalyst, (b) transmission electron microscopy (TEM) images of Bi_2O_3/TiO_2 S-scheme photocatalyst, and (c) photograph of floatable Bi_2O_3/TiO_2 S-scheme heterojunction photocatalyst. Reprinted with permission from Ref. [44], Copyright 2022, Wiley-VCH GmbH. (d) Synthesis process of In_2O_3@TiO_2 S-scheme heterojunction photocatalyst, (e) scanning electron microscopy (SEM) and (f) TEM images of In_2O_3@TiO_2 S-scheme heterojunction photocatalyst. Reprinted with permission from Ref. [45], Copyright 2023, Elsevier.

Gao *et al.* [67] also successfully constructed the dimensional-matched S-scheme heterojunction including TiO_2 nanosheets and Bi_2O_3 nanosheets through the two-step hydrothermal treatment. The dimensional-matched TiO_2/Bi_2O_3 S-scheme heterojunction photocatalyst not only possesses a large specific surface area, whereas it also prevents self-aggregation of TiO_2 nanosheets and Bi_2O_3 nanosheets as well as maintains its own morphological structure. Meanwhile, the tight two-dimensional (2D)/2D interfacial contact can also shorten the transport distance of the photo-induced carrier which prolongs the lifetime of the carrier. Besides, Wang *et al.* [45] successfully fabricated the In_2O_3@TiO_2 hollow structure S-scheme heterojunction photocatalyst using the hydrothermal method (Fig. 3d). The distributed TiO_2 nanosheets with sequential orientation uniformly on the surface of hollow In_2O_3 nanotubes can be obtained (Fig. 3e, f), which bestows a larger specific surface area that improves adsorption capacity for reactants. In an innovative study, He *et al.* [68] synthesized the ternary S-scheme heterojunction by loading WO_3 and TiO_2 on 2D reduced graphene oxide (rGO). In the WO_3/TiO_2/rGO system, the introduction of rGO as the support matrix results in plentiful adsorption and catalytic sites. Meanwhile, the formation of the Schottky junction between rGO and TiO_2 can also effectively promote photo-induced electron separation and transfer.

TiO_2/metal chalcogenide S-scheme heterojunction photocatalysts

Except for metal oxides, the metal chalcogenides are also explored for constructing TiO_2-based S-scheme heterojunction photocatalysts [46–48]. Specifically, metal sulfides have received much attention because of their tunable band energy level, narrower bandgap, wide light absorption range, higher carrier concentration, and strong reduction ability [69–71]. The S 3p orbitals are used to form the VB in the metal sulfides, which have low electronegativity and large atomic radius in comparison with the O element [72,73]. This result shows that the metal sulfide has a lower VB potential and narrower bandgap, bestowing it to absorb visible light. However, metal chalcogenides present rapid photo-induced carrier recombination and severe photocorrosion, hindering their photocatalytic application [74,75]. Thus, the establishment of S-scheme heterojunction is recognized as the effective method in addressing these limitations to strengthen the photocatalytic performances of TiO_2 and metal chalcogenide.

For example, Yang *et al.* [46] prepared a novel TiO_2/In_2S_3 S-scheme heterojunction photocatalyst *via* the electrostatic spinning and subsequent hydrothermal treatment (Fig. 4a), which shows a unique core-shell structure with TiO_2 nanofibres as the core and In_2S_3 nanosheets as the shell (Fig. 4b, c). The slit-shaped pores can be acquired by network structure originated from interwoven nanofibers, resulting in a large specific surface area to expose more active sites. Furthermore, Park *et al.* [76] successfully constructed a polyhedral cage shape CoS@TiO_2 S-scheme heterojunction photocatalyst through the simple hydrothermal treatment. Due to its dissolution and light corrosion in the photochemical reaction, CoS microsheets can knit in the polyhedral cage and the shell with stable TiO_2 can wrap the cage to overcome the above drawbacks, which is conducive to building a durable catalyst to boost photocatalytic performance. Recently, Zhang *et al.* [47] synthesized a novel Ni_3Se_4/TiO_2 S-scheme heterojunction photocatalyst through the *in situ* hydrothermal treatment (Fig. 5a–c). Specifically, the Ni_3Se_4 nanoparticles immobilized on the surface of TiO_2 broaden the light-harvesting range, promote photo-induced carrier separation and transfer, and provide more reactive sites, thereby achieving prominent photocatalytic efficiency. Furthermore, the ternary metal chalcogenides have also been extensively studied for constructing TiO_2-based S-scheme heterojunction photocatalysts, e.g., Wang and co-authors [48] designed an S-scheme core-shell hollow sphere photocatalyst *via* using SiO_2 spheres as a template and then depositing $ZnIn_2S_4$ nanosheets on the surface of TiO_2 (Fig. 5d, e). By constructing TiO_2@$ZnIn_2S_4$ S-scheme heterojunction photocatalyst with hollow structure, it shows a tight contact interface and improves light reflection and scattering, implying the significantly inhibited photo-induced carrier recombination and improved light-harvesting ability.

Besides the aforementioned metal chalcogenides, the other TiO_2/metal chalcogenide S-scheme heterojunction photocatalysts have also been successfully synthesized, such as CdS [77], ZnS [78], $MoSe_2$ [79], and $Zn_{0.2}Cd_{0.8}S$ [80].

TiO_2/organic semiconductor S-scheme heterojunction photocatalysts

Generally, organic semiconductors have a π-conjugated backbone structure and strong π–π interaction, which are an emer-

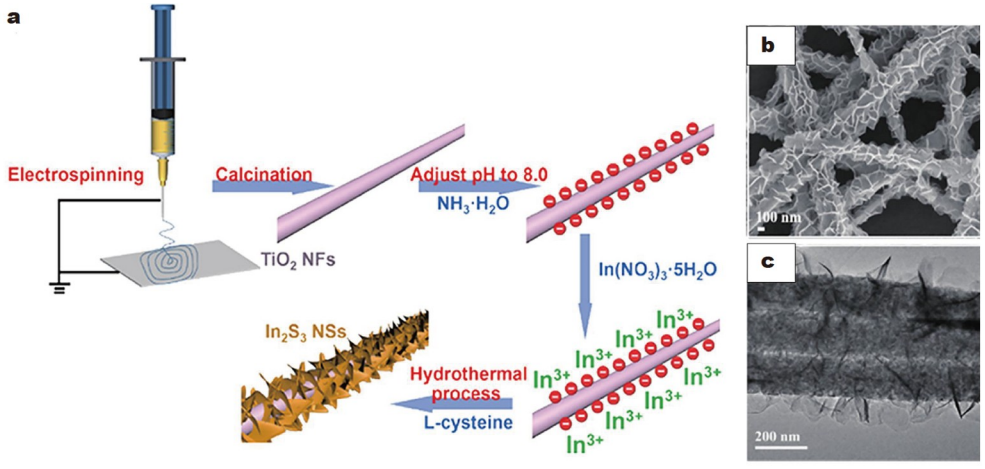

Figure 4 (a) Synthesis process of TiO_2/In_2S_3 S-scheme heterojunction photocatalyst, (b) SEM and (c) TEM images of TiO_2/In_2S_3 S-scheme heterojunction photocatalyst. Reprinted with permission from Ref. [46], Copyright 2021, Springer Nature.

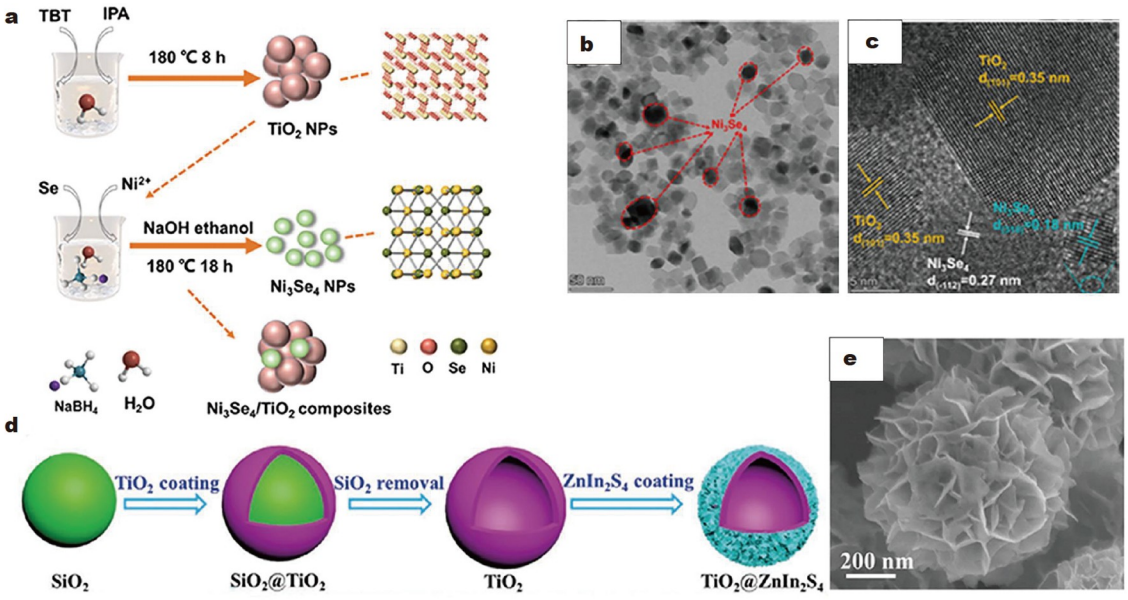

Figure 5 (a) Synthesis process of Ni_3Se_4/TiO_2 S-scheme heterojunction photocatalyst, (b) TEM and (c) high-resolution TEM (HRTEM) images of Ni_3Se_4/TiO_2 S-scheme heterojunction photocatalyst. Reprinted with permission from Ref. [47], Copyright 2023, American Chemical Society. (d) Synthesis process of $TiO_2@ZnIn_2S_4$, (e) SEM image of $TiO_2@ZnIn_2S_4$. Reprinted with permission from Ref. [48], Copyright 2021, Wiley-VCH GmbH.

ging class of metal-free photocatalysts [81,82]. By the appropriate molecular design and supramolecular assembly, organic semiconductors can usually be endowed with diversity and excellent photocatalytic performance [83,84]. Furthermore, the π-conjugated system of organic semiconductors also offers large carrier transport channels [50]. Nevertheless, the inadequate light-harvesting ability and severe photo-induced carrier recombination restrict its photocatalytic performance as with other photocatalysts [85]. Therefore, constructing TiO_2/organic semiconductor S-scheme heterojunction photocatalysts are identified as a potential method to boost photocatalytic performance.

For instance, Bi *et al.* [49] constructed the 0D/2D S-scheme heterojunction photocatalyst using the multi-step assembly strategy, which includes the vacancy defective TiO_2 (TiO_2-OV) quantum dots (QDs) loaded on 2D g-C_3N_4 nanosheets (Fig. 6a). Notably, TiO_2-OV QDs with abundant oxygen vacancies and uniform size can be obtained *via* a continuous supercritical water flow reaction and followed by heat treatment in N_2 atmosphere at different temperature. The as-obtained TiO_2-OV QDs/g-C_3N_4 enhances the interfacial charge transfer and offers abundant surface uncoordinated sites for photocatalytic reaction. Furthermore, inspired by the high light transmittance and fast gas fluidity from forest, Wang *et al.* [86] synthesized a forest-like TiO_2/g-C_3N_4 S-scheme heterojunction photocatalyst through the chemical oxidation and vapor deposition polymerization (Fig. 6b). In the hierarchical S-scheme thin film photocatalyst, the g-C_3N_4 can be loaded on TiO_2 nanowire arrays that grow on the surface of titanium foil. As a result, the unique structure with TiO_2 nanowire arrays as tree trunks and g-C_3N_4 as tree leaves possesses abundant active sites and efficient mass transport channels as well as high light utilization, resulting in the boosted photocatalytic performance. Besides, Meng *et al.* [87] developed a hollow core-shell spheres S-scheme heterojunction photocatalyst by modifying polydopamine (PDA) on the surface of a TiO_2 hollow sphere (Fig. 7a–c). The reasonable hollow structure design coordinated with the S-scheme heterojunction can broaden the light absorption range, improve the CO_2 adsorption ability, and achieve an excellent spatial separation and migration of photo-induced carrier. Recently, a novel TiO_2@COF (BTTA, 1,3,5-benzenetricarboxaldehyde (BT) and 4,4′,4″-(1,3,5-triazine-2,4,6-triyl) trianiline (TA)) S-scheme heterojunction photocatalysts have also been obtained by growing BTTA on the outermost layer of TiO_2 nanofibres (Fig. 7d) [50]. The innovative encapsulation of porous and ultra-thin BTTA endows the photocatalyst system with plentiful active sites and robust light-harvesting capacity. Moreover, the TiO_2/BTTA S-scheme heterojunction and π-conjugated system of BTTA contribute to the separation and shorten the transport distance of the photo-induced carrier.

TiO_2/other semiconductor S-scheme heterojunction photocatalysts Besides the aforementioned photocatalytic systems, the other semiconductors have also been explored to construct TiO_2-based S-scheme heterojunction photocatalysts, e.g., MOF [51], metal oxysalt [88], perovskite [52,89], and metal phosphide [20,90]. As a class of porous crystalline molecular materials, MOF possesses high porosity, sufficient visible light-harvesting ability, and component tunability. And, the special structure between metal ions and organic ligands can be exploited to provide a channel for the transfer of photo-induced carrier [91–93]. Due to versatile elemental compositions, tunable band gaps, and stable physicochemical properties, metal oxysalt and perovskite have attracted widespread attention in the field of photocatalysis [94–96]. Furthermore, metal phosphide possesses more high intrinsic activity, especially for hydrogen evolution reaction, which is mainly the reason that P atoms with negative charge can capture protons to drive hydrogen generation kinetics [20,97]. However, the inadequacy of a single semiconductor in the field of photocatalysis is also usually demonstrated in these photocatalysts. Constructing an S-scheme heterojunction is an effective method to boost the photocatalytic performances of TiO_2 and other

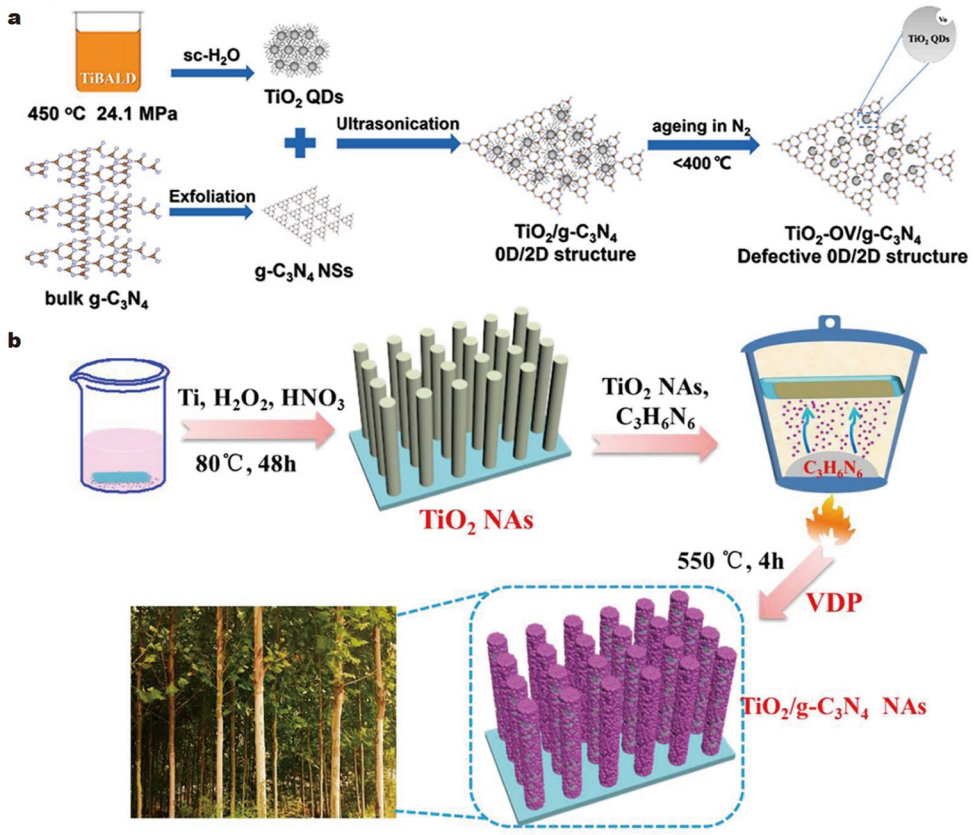

Figure 6 (a) Synthesis process of TiO_2-OV QDs/g-C_3N_4 S-scheme heterojunction photocatalyst. Reprinted with permission from Ref. [49], Copyright 2022, Elsevier. (b) Synthesis process of TiO_2/g-C_3N_4 S-scheme heterojunction photocatalyst. Reprinted with permission from Ref. [86], Copyright 2022, Elsevier.

semiconductors.

For instance, Zhu *et al.* [51] reported an ultrathin fluorine (F)-doped TiO_2(B) nanosheets *in situ* anchored on the surface of hierarchical cog wheel-shaped NH_2-MIL-53(Al) (NM(Al)) to synthesize the NM(Al)/F-TiO_2(B) S-scheme heterojunction photocatalyst by the hydrothermal method (Fig. 8a). The NM (Al) exhibits a cogwheel-like structure with the size of about 2.5 μm (Fig. 8b). Notably, the ultrathin F-TiO_2(B) nanosheets are introduced into the photocatalyst preparation system, which is closely bonded with NM(Al) (Fig. 8c). Benefitting from F-doped TiO_2(B) and an intimate contact interface between them, the reasonable heterojunction extends light absorption range and shortens the carrier diffusion distance, thereby acquiring the outstanding photocatalytic performance. Furthermore, Zhang *et al.* [88] also successfully fabricated an efficient S-scheme heterojunction photocatalyst based on Ti^{3+} self-doped black TiO_{2-x} mesoporous nanospheres and BiOI nanosheets *via* the hydrothermal treatment (Fig. 9a). From the TEM image of TiO_{2-x}/BiOI (Fig. 9b), it can be seen that the disk-like BiOI nanosheets are easier to load on TiO_{2-x} mesoporous nanospheres, which is mainly due to the rough surface of TiO_{2-x}. The constructed TiO_{2-x}/BiOI S-scheme heterojunction photocatalyst improves the light utilization and speeds up the photo-inducted carrier separation and transfer. Recently, Zhao *et al.* [89] reported an efficient and recyclable thin-film S-scheme heterojunction photocatalyst by growing piezoelectric material $BaTiO_3$ on TiO_2 nanorod arrays through the hydrothermal treatment. In the $BaTiO_3$/TiO_2 S-scheme heterojunction photocatalyst system, the unique piezoelectric property of $BaTiO_3$, matching energy band structure between them, and thin-film state are contributed to accelerate photo-induced carrier separation and transfer as well as recyclability of photocatalyst. Besides, Dong *et al.* [52] constructed the $CsPbBr_3$ QDs@ mesoporous TiO_2 (MTB) S-scheme heterojunction photocatalyst (Fig. 9c, d). Owing to the special morphological structure, $CsPbBr_3$ QDs are easily embedded into the pores of TiO_2 to ensure stability. As a result, the rational design can provide more active sites, shorten the photo-inducted carrier diffusion distance, and enhance the chemical stability of $CsPbBr_3$ QDs. Chen *et al.* [20] also fabricated the P and C co-doped Co_2P/black TiO_2 (Co_2P/PC-b-TiO_2) S-scheme heterojunction photocatalyst *via* a combination of hydrothermal and calcination methods. The *in situ* formed Co_2P nanoparticles can be extensively coordinated with b-TiO_2, ensuring a tight contact interface. Notably, the P and C dopants can inhibit the anatase-to-rutile phase transformation of TiO_2 and fulfill the bulk oxygen defects to restrain the photo-induced carrier recombination, respectively. In the Co_2P/PC-b-TiO_2 S-scheme heterojunction system, the intimately coupled heterointerface and strong internal electric field are contributed to boost the photocatalytic performance.

APPLICATIONS OF TiO_2-BASED S-SCHEME HETEROJUNCTION PHOTOCATALYSTS IN ENERGY CONVERSION AND ENVIRONMENTAL REMEDIATION

Photocatalytic hydrogen evolution

Hydrogen (H_2), a clean energy source, is deemed to be an ideal

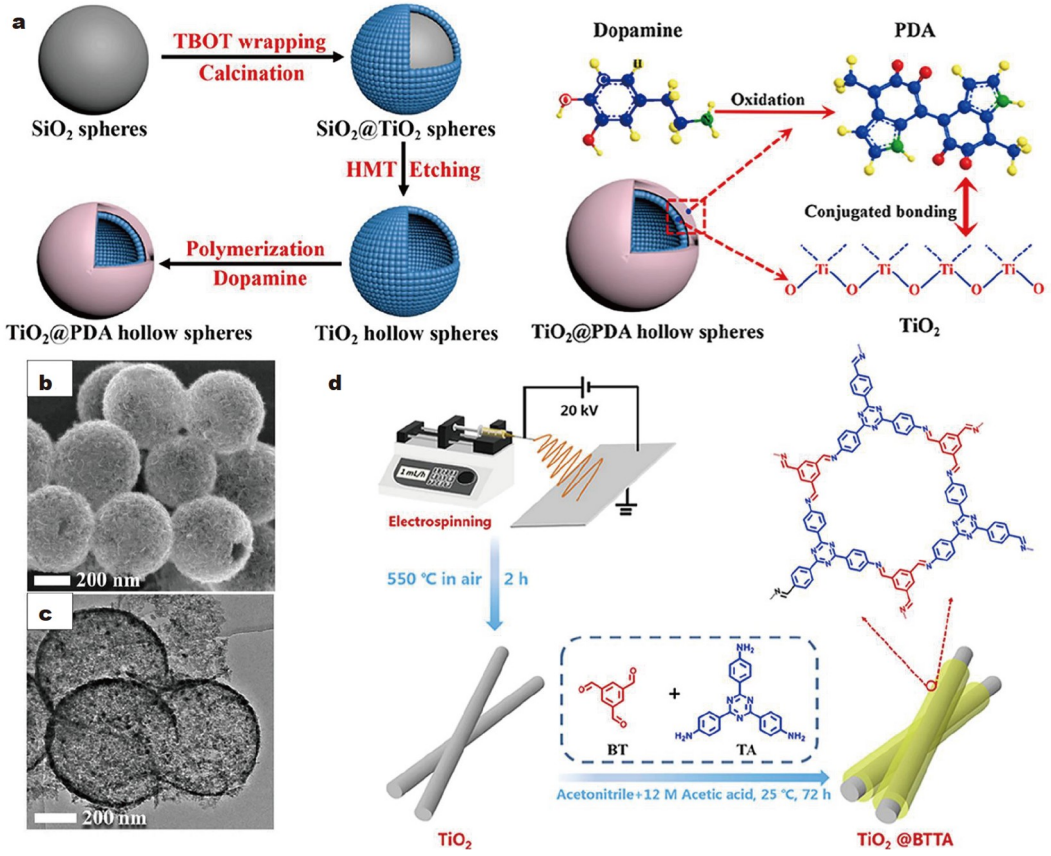

Figure 7 (a) Synthesis process (left) and structural diagram (right) of TiO_2@PDA S-scheme heterojunction photocatalyst, (b) SEM and (c) TEM images of TiO_2@PDA S-scheme heterojunction photocatalyst. Reprinted with permission from Ref. [87], Copyright 2021, Elsevier. (d) Synthesis process of TiO_2@BTTA S-scheme heterojunction photocatalyst. Reprinted with permission from Ref. [50], Copyright 2023, Elsevier.

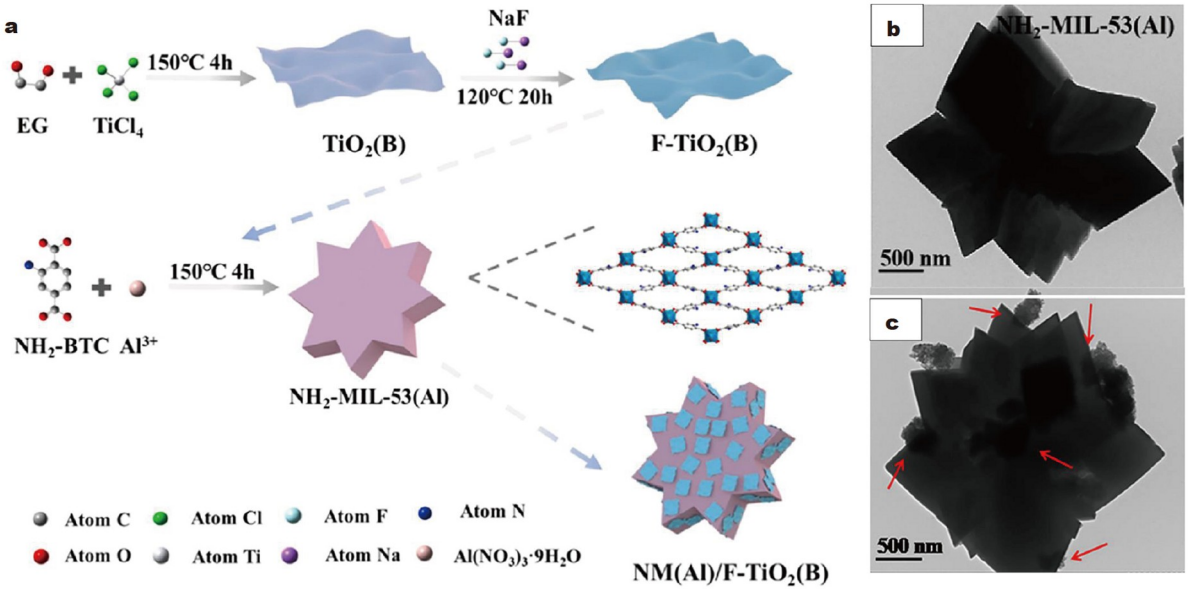

Figure 8 (a) Synthesis process of NM(Al)/F-TiO_2(B) S-scheme heterojunction photocatalyst, TEM images of (b) NM(Al) and (c) NM(Al)/F-TiO_2(B). Reprinted with permission from Ref. [51], Copyright 2023, Elsevier.

energy medium to substitute traditional fossil fuels because of the high energy density (120 MJ kg^{-1}) [98–100]. Photocatalytic water splitting has been recognized as an effective strategy for H_2 evolution [101–103]. According to the photocatalytic water splitting reaction, the reaction process is a thermodynamically uphill that requires the semiconductor with a minimum band-

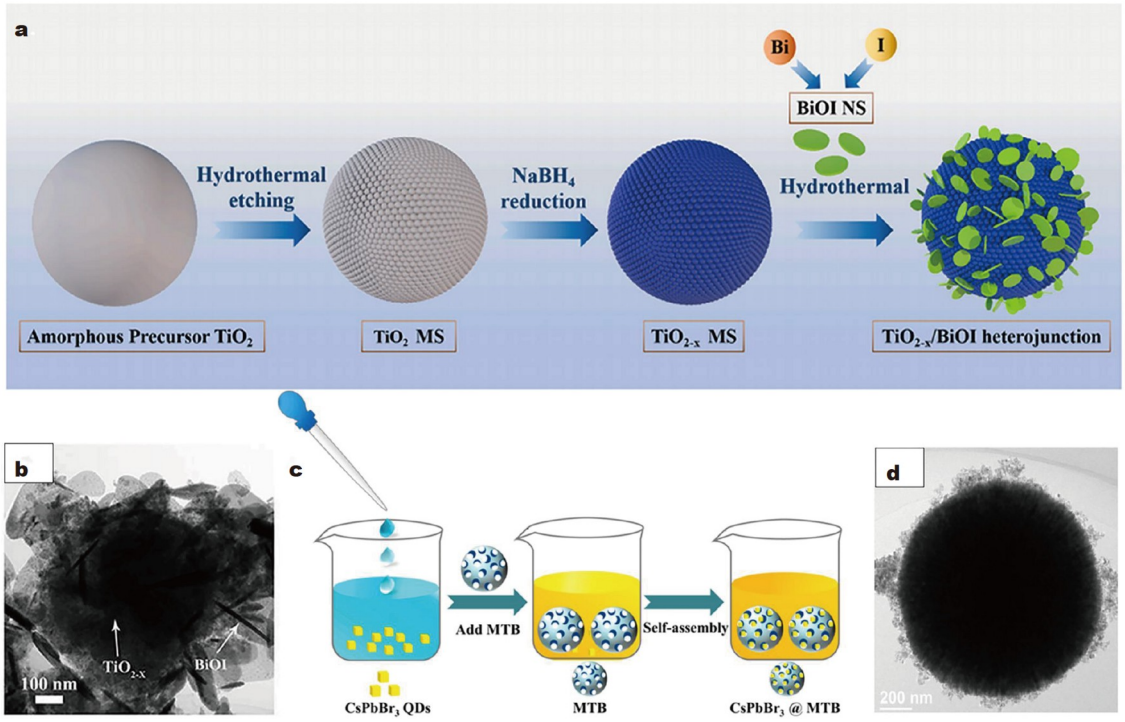

Figure 9 (a) Synthesis process of TiO_{2-x}/BiOI S-scheme heterojunction photocatalyst, (b) TEM image of TiO_{2-x}/BiOI. Reprinted with permission from Ref. [88], Copyright 2022, Elsevier. (c) Synthesis process of $CsPbBr_3$ QDs@MTB S-scheme heterojunction photocatalyst, (d) TEM image of $CsPbBr_3$ QDs@MTB. Reprinted with permission from Ref. [52], Copyright 2022, Elsevier.

gap energy of 1.23 eV to overcome the Gibbs free energy of 237.2 kJ mol^{-1} [104–106]. As a result, the CB potential deserves a more negative relative to water reduction potential (H^+/H_2, 0 eV *vs.* NHE), while the VB potential needs to be more positive in comparison with water oxidation potential (H_2O/O_2, 1.23 eV *vs.* NHE) [105,107]. Yet, a single TiO_2 is insufficient to acquire the condition. In this case, the potential requirements can be satisfied by constructing TiO_2-based S-scheme heterojunction photocatalysts to achieve an outstanding photocatalytic H_2 evolution performance.

For example, Li *et al.* [108] constructed the 1D/2D TiO_2/$ZnIn_2S_4$ S-scheme heterojunction photocatalyst for photocatalytic H_2 evolution. By the X-ray photoelectron spectroscopy (XPS) characterization analysis with and without light illumination (Fig. 10a, b), note that the *in situ* and *ex-situ* XPS peaks of Ti 2p and Zn 2p in the TiO_2/$ZnIn_2S_4$ exhibit opposite shift direction in comparison with TiO_2 and $ZnIn_2S_4$, suggesting that electrons transfer from TiO_2 to $ZnIn_2S_4$, which is in good agreement with S-scheme heterojunction mechanism. Thus, the photocatalytic H_2 evolution rate (6.03 mmol g^{-1} h^{-1}) of optimal TiO_2/$ZnIn_2S_4$ is 3.7 and 2 folds than bare TiO_2 and $ZnIn_2S_4$. Meanwhile, the apparent quantum yield (AQY) of photocatalyst can reach 10.5% under 365 nm irradiation. Furthermore, Gao *et al.* [67] reported a dimensional-matched TiO_2/Bi_2O_3 photocatalyst for H_2 evolution. In the calculated Fermi energy levels and work functions of TiO_2 (001) and Bi_2O_3 (001) (Fig. 10c, d), the Fermi energy level of TiO_2 is higher compared to Bi_2O_3, indirectly confirming the possibility for forming S-scheme heterojunction. By combining the electron paramagnetic resonance (EPR) spectra of DMPO-·O_2^- adduct (Fig. 10e), it is worth noting that no DMPO-·O_2^- signal of Bi_2O_3 is detected because CB potential of Bi_2O_3 is lower than the reduction potential of O_2/·O_2^-, while DMPO-·O_2^- signal of TiO_2/Bi_2O_3 achieves significantly enhanced compare to TiO_2, suggesting that TiO_2/Bi_2O_3 can produce more ·O_2^-. These results follow the S-scheme heterojunction mechanism in the TiO_2/Bi_2O_3 system. The constructed S-scheme heterojunction photocatalyst obtains the photocatalytic H_2 evolution rate of 12.08 mmol g^{-1} h^{-1} under simulated sunlight irradiation (Fig. 10f). Recently, Bi *et al.* [49] also successfully utilized the vacancy defective TiO_2 QDs to couple 2D g-C_3N_4 nanosheets for constructing TiO_2-OV QDs/g-C_3N_4 S-scheme heterojunction photocatalyst. By density functional theory (DFT) calculation, the adsorption, reaction pathway, and optimized geometric structure of H_2O molecules on the TiO_2 QDs/g-C_3N_4 and TiO_2-OV QDs/g-C_3N_4 are studied in the photocatalytic H_2 evolution reaction (Fig. 11a, b). The results display that the defect engineering improves the adsorption and dissociation of H_2O molecules on the TiO_2-OV QDs/g-C_3N_4 and the Volmer reaction tends to be the TiO_2-OV QDs/g-C_3N_4. In this case, the optimal TiO_2-OV QDs/g-C_3N_4 exhibits excellent photocatalytic H_2 evolution rate of 1.10 mmol g^{-1} h^{-1} (Fig. 11c). The enhanced photocatalytic performance is also attributed to the formed S-scheme heterojunction that improves photo-induced carrier separation and transfer and reserves strong redox ability (Fig. 11d). More detailed TiO_2-based S-scheme heterojunction photocatalysts for H_2 evolution performances are displayed in Table 1 [20,49,67,68,77,78,80,88,90,108–113].

Photocatalytic CO_2 reduction

With the rapid development of human society, massive CO_2 in the atmosphere is emitted through the excessive consumption of fossil fuels, leading to extreme weather and the greenhouse effect, so it is urgent to explore the reasonable utilization of CO_2 [114,115]. Similar to the photosynthesis process in nature,

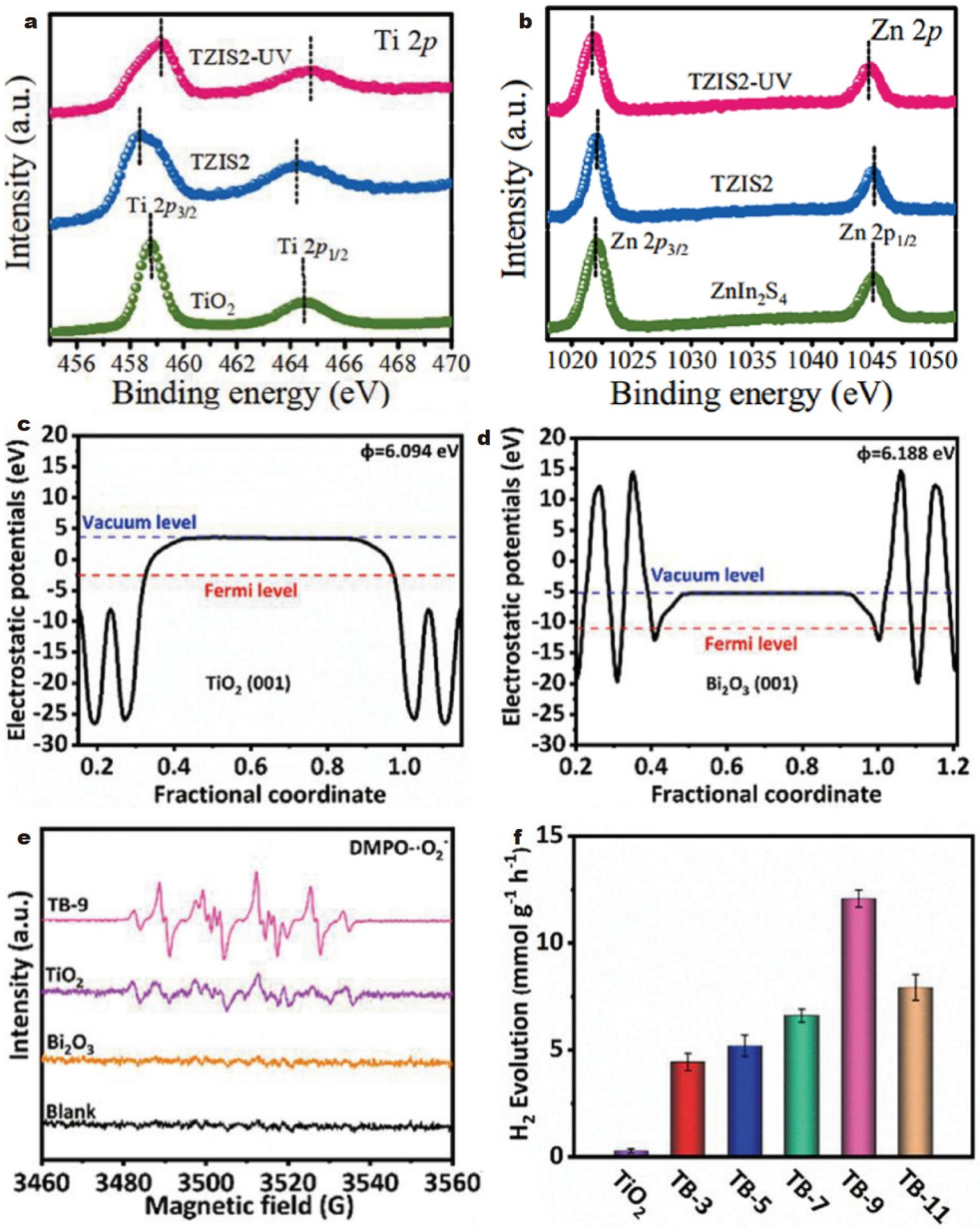

Figure 10 XPS spectra of (a) Ti 2p, (b) Zn 2p over TiO_2, $ZnIn_2S_4$, and $TiO_2/ZnIn_2S_4$ with and without light illumination. Reprinted with permission from Ref. [108], Copyright 2022, Elsevier. Calculated Fermi energy levels and work functions of (c) TiO_2 (001) and (d) Bi_2O_3 (001), (e) EPR spectra of DMPO-·O_2^- adduct over TiO_2, Bi_2O_3, and TiO_2/Bi_2O_3 under illumination, (f) photocatalytic H_2 evolution rates over different samples. Reprinted with permission from Ref. [67], Copyright 2022, Elsevier.

photocatalytic CO_2 reduction is considered as a clean conversion technology to convert CO_2 into high-value chemical fuels, including CO, CH_4, CH_3OH, HCOOH, and other hydrocarbon fuels [116–118]. Therefore, photocatalytic CO_2 reduction can significantly reduce CO_2 concentrations and simultaneously produce low-carbon fossil fuels, which offers a potential solution to address the climate issue and energy shortage [119–121]. However, CO_2 has a stable molecular structure, implying that the photocatalytic CO_2 reduction reaction requires an extremely high energy to achieve the cleavage of C=O bond (750 kJ mol^{-1}) [122,123]. Moreover, the thermodynamic uphill reaction and complex multi-electronic process of CO_2 reduction require the strong redox ability along with effective separation of the photo-induced carrier to furnish sufficient driving force in the photocatalytic system [36,124]. By constructing TiO_2-based S-scheme heterojunction photocatalysts, it can not only meet the strict energy band structure requirements but also achieve a strong redox ability. This result indicates that S-scheme heterojunction is more conducive to photocatalytic CO_2 reduction reaction. As shown in Table 2 [43,48,52,87,125–127], the TiO_2-based S-scheme heterojunction photocatalysts for CO_2 reduction performances and products are summarized in detail.

For instance, Wang *et al.* [48] have shown that converting CO_2 into CO, CH_3OH, and CH_4 can be obtained by a core-shell TiO_2@$ZnIn_2S_4$ S-scheme heterojunction photocatalyst. By the EPR spectra of $\cdot O_2^-$ and ·OH measurement (Fig. 12a, b), it is worth noting that the signal intensities of DMPO-·OH and DMPO-·O_2^- are evidently stronger than TiO_2 and $ZnIn_2S_4$,

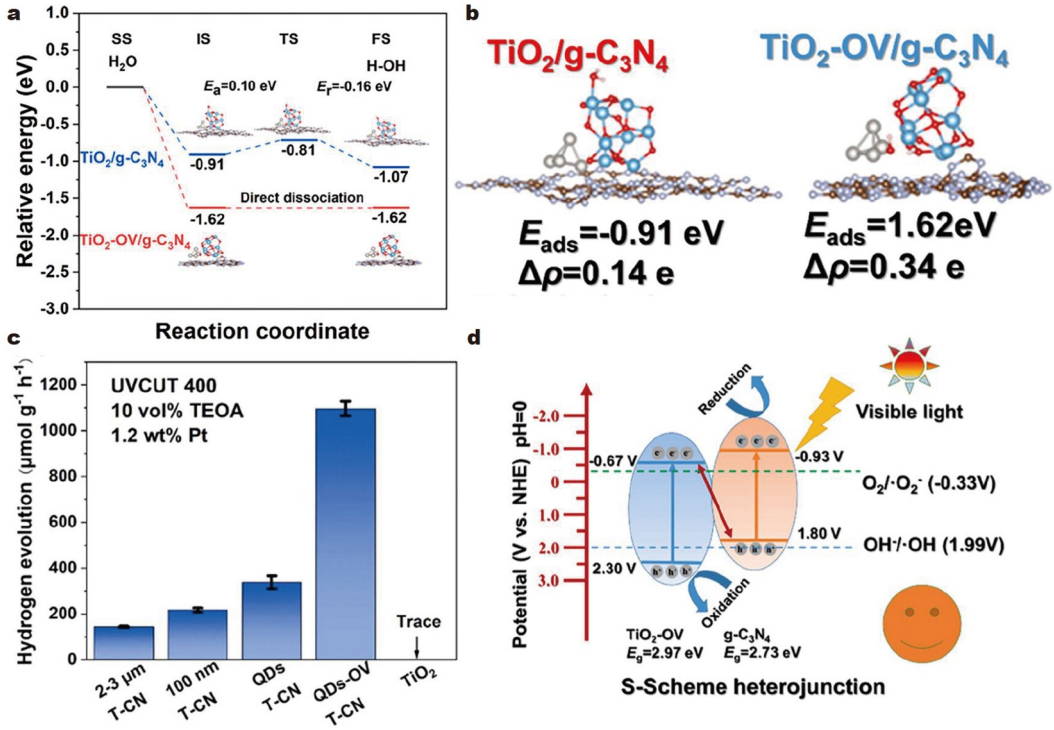

Figure 11 (a) Adsorption and reaction pathway of H_2O molecules on the TiO_2/g-C_3N_4 and TiO_2-OV/g-C_3N_4; (b) optimized geometric structures of H_2O molecule adsorption on TiO_2/g-C_3N_4 and TiO_2-OV/g-C_3N_4; (c) photocatalytic H_2 evolution rates over different samples; (d) schematic illustration for photo-induced carrier transfer route over TiO_2-OV/g-C_3N_4 S-scheme heterojunction photocatalyst. Reprinted with permission from Ref. [49], Copyright 2022, Elsevier.

Table 1 Detailed H_2 evolution performances over TiO_2-based S-scheme heterojunction photocatalysts

S-scheme heterojunction	Sacrificial agent	H_2 evolution rate (mmol g^{-1} h^{-1})	Enhancement factor *vs.* TiO_2	AQY	Ref.
TiO_2/Bi_2O_3	TEOA	12.08	43.8	–	[67]
WO_3/TiO_2/rGO	Methanol	0.25	3.5	1.4% (365 nm)	[68]
ZnS/TiO_2	Na_2SO_3, Na_2S	5.50	38.8	–	[78]
$CdS/Bi/TiO_2$	Na_2SO_3, Na_2S	0.67 mmol cm^{-1} h^{-1}	–	–	[77]
Co_9S_8/TiO_2	TEOA	0.40	13.2	–	[109]
$TiO_2/ZnIn_2S_4$	TEOA	6.03	3.7	10.5% (365 nm)	[108]
TiO_2/Ni-$Zn_{0.2}Cd_{0.8}S$	–	4.55	–	16.6% (365 nm)	[80]
TiO_2-OV QDs/g-C_3N_4	TEOA	1.10	–	–	[49]
Ni@TiO_2/g-C_3N_4	TEOA	0.13	10.3	15.0% (420 nm)	[110]
TiO_{2-x}/TpPa-1-COF	Sodium ascorbate	15.33	10.5	6.7% (420 nm)	[111]
TiO_{2-x}/BiOI	Methanol	0.79	3.0	4.46% (365 nm)	[88]
$TiO_2/In_{0.5}WO_3$/rGO	Glycerol	0.31	12.0	15.6% (365 nm)	[112]
P-$CuWO_4/TiO_2$	TEOA	6.17	26.0	–	[113]
Co_2P/PC-b-TiO_2	TEOA	1.53	–	12.5% (420 nm)	[20]
Cu_3P/TiO_2	Methanol	5.83	7.3	–	[90]

verifying that the photo-induced carrier transfer process is in good agreement with S-scheme heterojunction mechanism (Fig. 12c). Because of the unique hollow structure and S-scheme heterojunction, the optimized TiO_2@$ZnIn_2S_4$ presents markedly improved photocatalytic performance with the total CO_2 photoreduction conversion rate of 18.32 μmol g^{-1} h^{-1} that is superior to pristine $ZnIn_2S_4$ and TiO_2 (Fig. 12d). Additionally, Meng *et al.* [87] constructed a TiO_2@PDA S-scheme heterojunction photocatalyst for photocatalytic CO_2 reduction. The as-obtained photocatalyst shows an outstanding CO_2 reduction selectivity with the CH_4 yield of 1.50 μmol g^{-1} h^{-1}, achieving nearly 5 times higher than pristine TiO_2. As a result, the boosted

Table 2 Detailed CO_2 reduction performances over TiO_2-based S-scheme heterojunction photocatalysts

S-scheme heterojunction	Reduction products	Yield ($\mu mol\ h^{-1}\ g^{-1}$)	Enhancement factor *vs.* TiO_2	Ref.
MoS_2/TiO_2	CO, CH_4	36.30, 108.80	40.3, –	[126]
$TiO_2@ZnIn_2S_4$	CO, CH_4, CH_3OH	9.28, 4.26, 4.78	3.4, 10.1, 5.0	[48]
$TiO_2/C_3N_4/Ti_3C_2$	CO, CH_4	4.39, 1.20	3.0, 8.0	[43]
TiO_2@PDA	CH_4	1.50	5.0	[87]
TiO_2@CoNi-MOF	CH_4	41.65	–	[127]
$TiO_2@Bi_2MoO_6$	CO	30.66	4.0	[125]
$CsPbBr_3$ QDs@TiO_2	CO	145.28	4.6	[52]

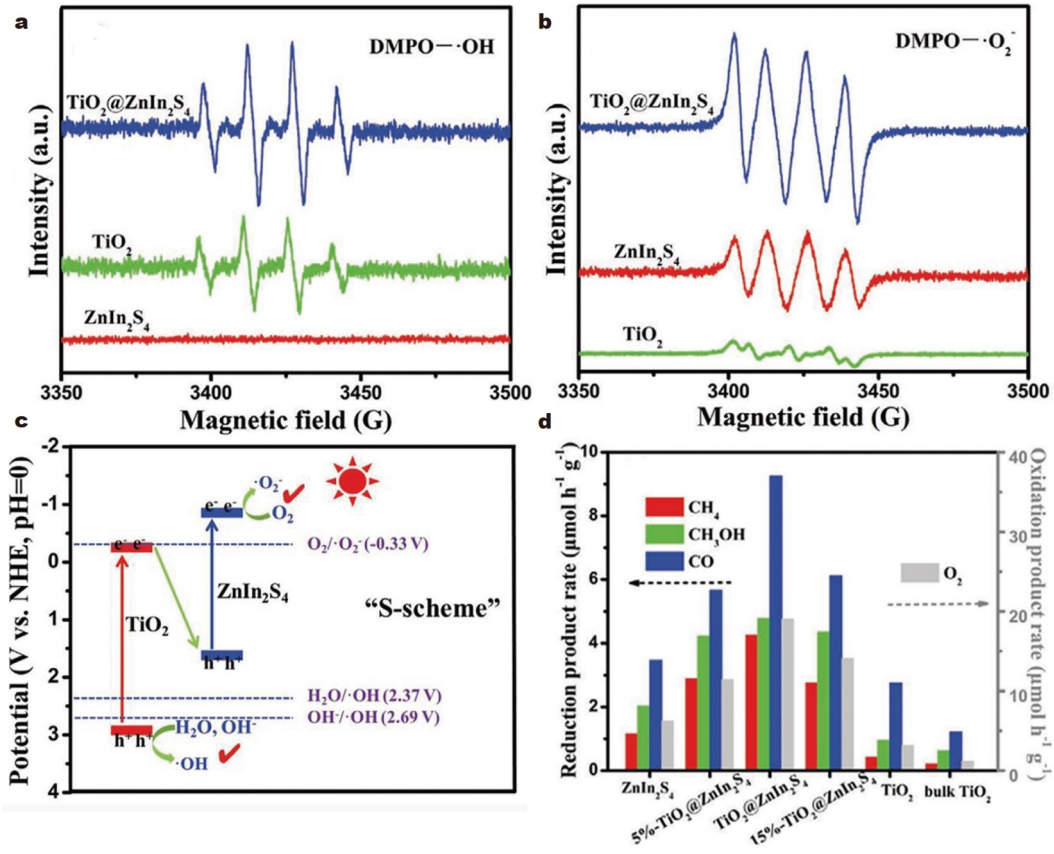

Figure 12 EPR spectra of (a) ·OH and (b) $\cdot O_2^-$ trapping tests of TiO_2, $ZnIn_2S_4$, and $TiO_2@ZnIn_2S_4$ under illumination; (c) schematic illustration for photo-induced carrier transfer route over $TiO_2@ZnIn_2S_4$; (d) yields of CO_2 reduction products over different samples. Reprinted with permission from Ref. [48], Copyright 2021, Wiley-VCH GmbH.

photocatalytic performance can be credited to the S-scheme heterojunction construction that improves the efficient photo-induced carrier separation and migration, and provides a strong redox ability (Fig. 13a). Recently, Ren *et al.* [125] also prepared the hollow $TiO_2@Bi_2MoO_6$ S-scheme heterojunction photocatalyst for photocatalytic CO_2 reduction into CO. By combining the calculated Fermi energy levels and work functions of TiO_2 (101) and Bi_2MoO_6 (131), the photo-induced electrons in the TiO_2 are quenched with holes in the Bi_2MoO_6, thereby the effective photo-induced carrier with strong redox ability is retained (Fig. 13b–d). In this case, the S-scheme heterojunction photocatalyst shows a higher CO yield (30.66 $\mu mol\ g^{-1}\ h^{-1}$), far exceeds that of pure TiO_2 and Bi_2MoO_6.

Photocatalytic H_2O_2 production

Hydrogen peroxide (H_2O_2), as a clean oxidizer, has been extensively employed in chemical synthesis, disinfection, wastewater treatment, and fuel cells [128–130]. Generally, the commercially available H_2O_2 is mainly prepared *via* anthraquinone oxidation that requires high energy consuming and produces toxic by-products [131,132]. Conversely, photocatalytic technology is considered a mild and environment-friendly method to realize the H_2O_2 production, which only requires O_2, H_2O, and solar energy as the raw materials [133–135]. To date, the mechanism of photocatalytic H_2O_2 production is generally accepted by a two-electron O_2 reduction reaction or two-electron water oxidation reaction [136–138]. No matter what kind of

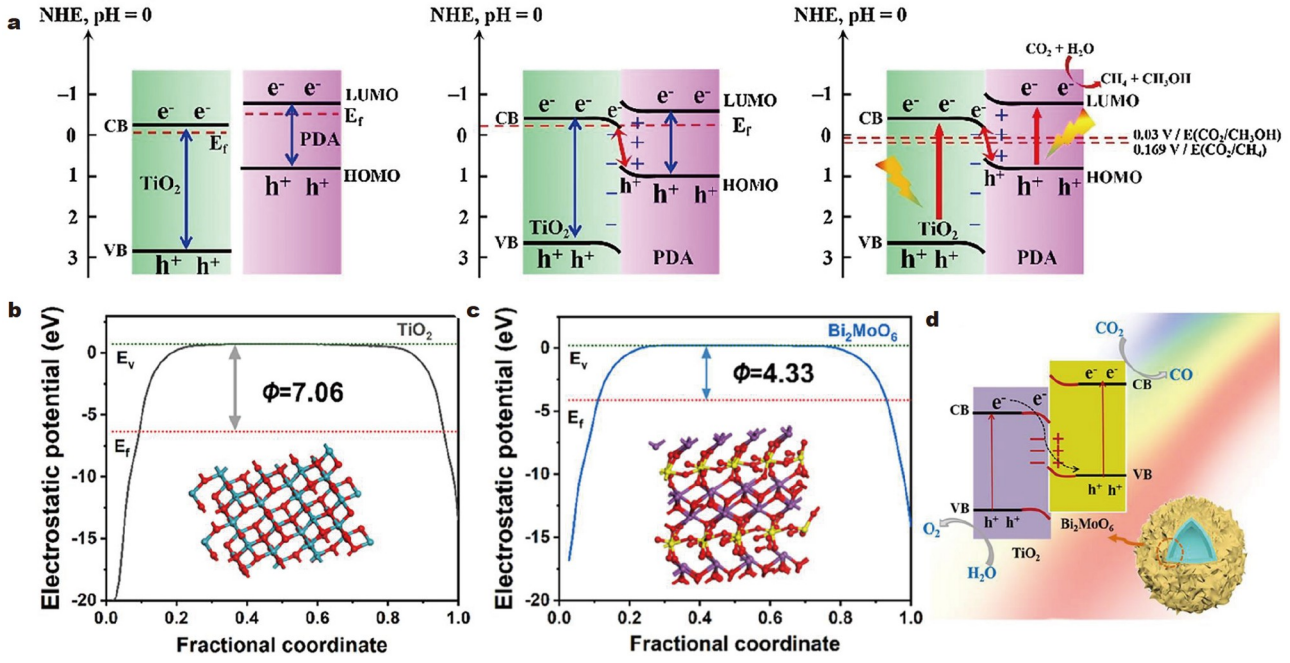

Figure 13 (a) Schematic illustration of S-scheme heterojunction mechanism between TiO_2 and PDA. Reprinted with permission from Ref. [87], Copyright 2021, Elsevier. Calculated Fermi energy levels and work functions of (b) TiO_2 (101) and (c) Bi_2MoO_6 (131), (d) proposed photocatalytic CO_2 reduction mechanism of TiO_2@Bi_2MoO_6. Reprinted with permission from Ref. [125], Copyright 2023, Elsevier.

photocatalytic mechanism, the photocatalyst has put forward strict requirements with strong redox ability. Thus, the TiO_2-based S-scheme heterojunction photocatalysts can be widely exploited for H_2O_2 production.

For instance, He *et al.* [44] developed the floatable TiO_2/Bi_2O_3 S-scheme heterojunction photocatalyst for photocatalytic H_2O_2 production. Due to the unique floatable property, the floatable S-scheme heterojunction photocatalyst is easier to absorb light to produce more photo-induced carrier and oxygen can quickly spread to solid-liquid interface to participate in photocatalytic H_2O_2 production in the air-liquid-solid system (Fig. 14a). Furthermore, the femtosecond transient absorption (fs-TA) spectrum of TiO_2/Bi_2O_3 exhibits an attenuated peak at 395 nm and more distinct peak at 450 nm compared to TiO_2 (Fig. 14b, c), suggesting that the photo-induced electrons migrate from TiO_2 to Bi_2O_3. The result follows the S-scheme heterojunction mechanism. Under simulated sunlight irradiation, the optimal photocatalyst acquires a markedly improved photocatalytic H_2O_2 production performance (1.15 mmol L^{-1} h^{-1}), which is superior to bare TiO_2 and Bi_2O_3 (Fig. 14d). Thus, the synergistic effects of floatable property and S-scheme heterojunction are contributed to boost the photocatalytic performance. Additionally, Yang *et al.* [46] fabricated TiO_2/In_2S_3 S-scheme heterojunction photocatalyst with excellent H_2O_2 production performance (0.38 mmol L^{-1} h^{-1}). By the DFT calculation (Fig. 15a, b) and other characterization analysis, converting O_2 to H_2O_2 is a stepwise one-electron processes. And, In_2S_3 presents a strong interaction with O_2 compared to TiO_2, which is a reason that the photocatalytic activity of S-scheme heterojunction far exceeds that of TiO_2. Recently, Xia *et al.* [134] have grown TiO_2 nanocrystals on the inner walls of hollow resorcinol-formaldehyde (RF) resin nanocakes to construct TiO_2@RF S-scheme heterojunction photocatalyst. Such a hollow Janus core-shell structure design significantly improves the photo-induced carrier separation and active site exposure. Besides, Kelvin probe force microscopy (KPFM) has been ascertained the interfacial charge transfer behavior of TiO_2@RF, as shown in Fig. 15c–e. Notably, it can be seen that the significant difference in the surface potential signals presents under illumination and darkness, indicating that the photo-induced electrons can move from TiO_2 to RF. Under light irradiation and without a sacrificial agent, the TiO_2@RF S-scheme heterojunction photocatalyst exhibits the excellent photocatalytic H_2O_2 production rate up to 0.67 mmol L^{-1} h^{-1}. More detailed TiO_2-based S-scheme heterojunction photocatalysts for H_2O_2 production are displayed in Table 3 [44,46,50,131,134].

Pollutant degradation

With the rapid development of modern industry, the natural environment is being contaminated by the discharge of wastewater containing hazardous substances that cause a series of human health problems [139–141]. To address the problem, the photocatalytic technology has been extensively studied for degrading pollutants into non-toxic or low toxic substances through efficiently producing reactive oxygen species ($\cdot O_2^-$, ·OH, and h^+) [142,143]. In photocatalytic reaction, the electrons can interact with the dissolved O_2 in water to produce $\cdot O_2^-$, while the holes can oxidize with H_2O into ·OH [143,144]. As a results, the semiconductor photocatalyst is required to meet the thermodynamical conditions for the oxidation potential of $H_2O/\cdot OH$ (1.99 eV *vs.* NHE) and reduction potential of $O_2/\cdot O_2^-$ (−0.33 eV *vs.* NHE) [145,146]. Inspired by the unique photo-induced carrier transfer route, the photo-induced carrier in the TiO_2-based S-scheme heterojunction system can be effectively separated and reserves a strong redox ability that will participate in photocatalytic pollutant degradation. Table 4 [51,55,147–152]

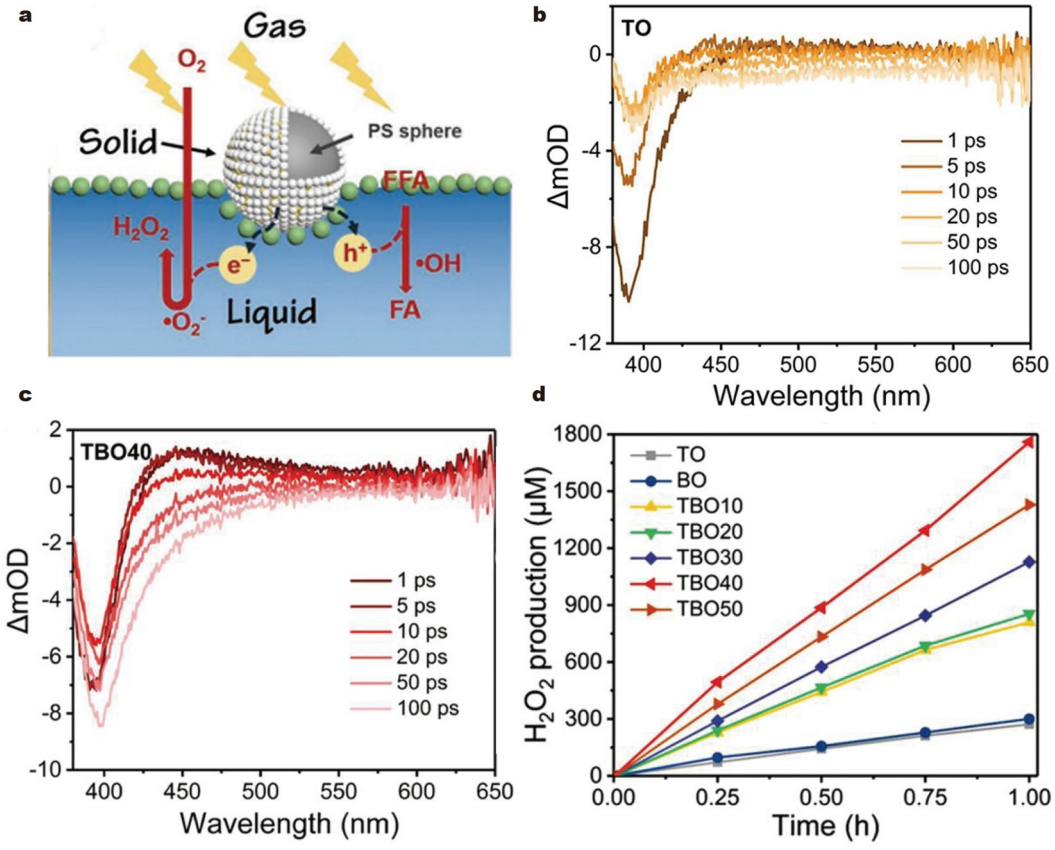

Figure 14 (a) Schematic illustration for photocatalytic reaction of TiO_2/Bi_2O_3 in the air-liquid-solid system, fs-TA spectra of (b) TiO_2 and (c) TiO_2/Bi_2O_3, (d) photocatalytic H_2O_2 production over different samples. Reprinted with permission from Ref. [44], Copyright 2022, Wiley-VCH GmbH.

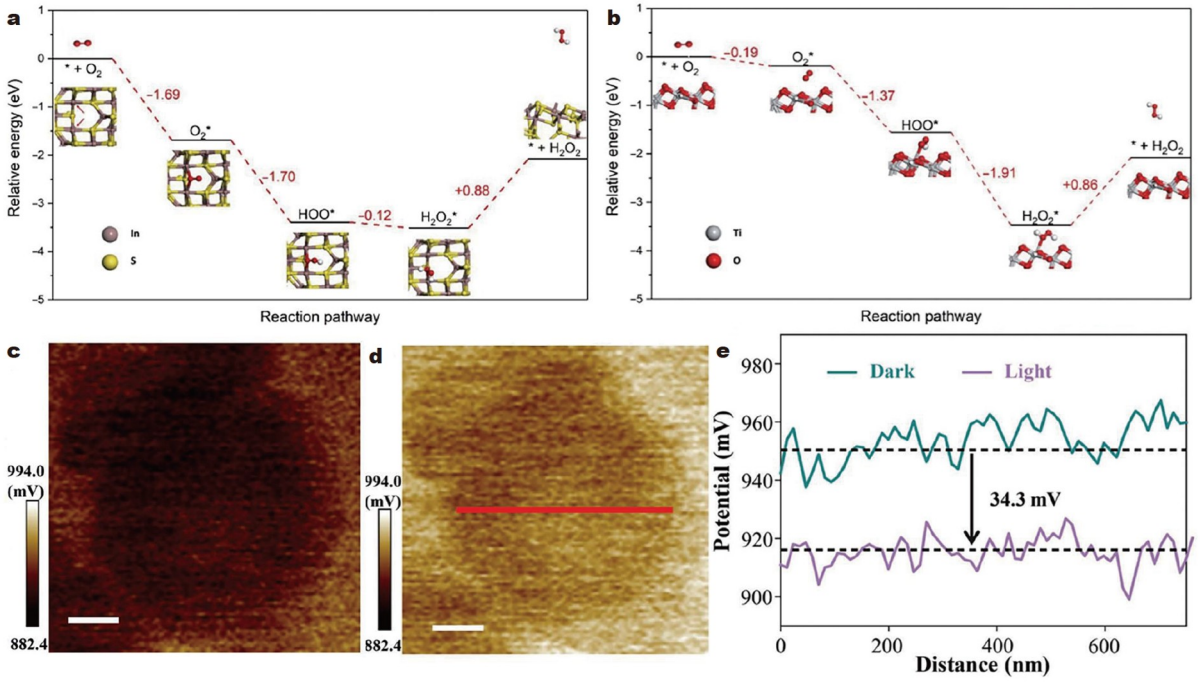

Figure 15 DFT calculation for free energy of O_2 conversion to H_2O_2 by (a) In_2S_3 (101) and (b) TiO_2 (101). Reprinted with permission from Ref. [46], Copyright 2021, Springer Nature. KPFM images of TiO_2@RF (c) with and (d) without light illumination and (e) the corresponding surface potentials. Reprinted with permission from Ref. [134], Copyright 2023, Wiley-VCH GmbH.

Table 3 Detailed H_2O_2 production performances over TiO_2-based S-scheme heterojunction photocatalysts

S-scheme heterojunction	Sacrificial agent	Yield (mmol L^{-1} h^{-1})	Enhancement factor *vs.* TiO_2	AQY (365 nm)	Ref.
TiO_2/Bi_2O_3	Furfuryl alcohol	1.15	3.8	1.25%	[44]
TiO_2/In_2S_3	Ethanol	0.38	5.4	3.42%	[46]
S-g-C_3N_4/TiO_2	–	0.43	133.0	0.61%	[131]
TiO_2@BTTA	Furfuryl alcohol	0.74	23.6	5.48%	[50]
TiO_2@RF	–	0.67	–	–	[134]

Table 4 Detailed pollutant degradation performances over TiO_2-based S-scheme heterojunction photocatalysts

S-scheme heterojunction	Application	Degradation efficiency	Enhancement factor *vs.* TiO_2	Ref.
Bi_2O_3/TiO_2	Phenol	45%/120 min	–	[148]
In_2S_3/TiO_2(B)	Tetracycline	97.3%/120 min	3.2	[149]
TiO_{2-x}/g-C_3N_4/CNFe	Atrazine	95.4%/30 min	4.5	[150]
Fe_3O_4/TiO_2/g-C_3N_4	U(VI) Sb(III)	93.0%/180 min 83.5%/180 min	–	[55]
SCN/TiO_2	Congo Red	95%/60 min	–	[147]
PDI/g-C_3N_4/TiO_2@Ti_3C_2	Atrazine	75%/60 min	–	[151]
NM(Al)/F-TiO_2(B)	Tetracycline	94.6%/120 min	2.3	[51]
Ag_3PO_4/TiO_2	Rhodamine B Phenol Tetracycline	100%/5 min 60%/15 min 100%/8 min	–	[152]

summarizes the latest developments in photocatalytic pollutant degradation over TiO_2-based S-scheme heterojunction photocatalysts.

For example, Wang *et al.* [147] used electrospinning and calcination methods to construct the uniformly distributed 1D nanostructure S-doped g-C_3N_4 (SCN)/TiO_2 S-scheme heterojunction photocatalyst for Congo Red degradation. By the *in situ* XPS (Fig. 16a, b) and other characterization analyses, it is seen that the photo-induced carrier immigration route follows the S-scheme heterojunction mechanism (Fig. 16c). Benefiting from the introduction of the S element along with the construction of S-scheme heterojunction, the optimal photocatalyst demonstrates excellent photocatalytic Congo Red degradation efficiency as high as 95% after irradiation for 60 min (Fig. 16d), which is superior to bare SCN and TiO_2. Furthermore, He *et al.* [148] reported a hierarchical Bi_2O_3/TiO_2 fibrous S-scheme heterojunction photocatalyst for phenol degradation. Due to its hierarchical fibrous structure and S-scheme heterojunction mechanism, achieving a phenol photodegradation efficiency of 45% under simulated sunlight. Recently, Zhu *et al.* [51] fabricated NM(Al)/F-TiO_2(B) S-scheme heterojunction photocatalyst, the photocatalytic mechanism of NM(Al)/F-TiO_2(B) S-scheme heterojunction photocatalyst for tetracycline photodegradation was also demonstrated by characterization analyses and experimental results. As shown in Fig. 17a, the establishment of S-scheme heterojunction greatly improves light absorption, boosts spatial photo-induced carrier separation and migration, and retains the strong redox capacity to produce more $\cdot O_2^-$ and ·OH active species. Thus, the NM(Al)/F-TiO_2(B) exhibits a remarkable photocatalytic tetracycline degradation performance with an efficiency of 94.6%. Besides, the team also constructed a hierarchical 3D/2D In_2S_3/TiO_2(B) S-scheme heterojunction photocatalyst [149]. In the photocatalytic degradation of tetracycline, the mainly active species towards tetracycline photodegradation are $\cdot O_2^-$ and ·OH *via* the electron spin resonance spectra (Fig. 17b, c). In this case, the kinetic constant for tetracycline photodegradation of the optimal S-scheme heterojunction photocatalyst reaches 0.029 min^{-1}, which is about 9.7 and 5.8 times of bare TiO_2 and Bi_2O_3, respectively.

CONCLUSIONS AND OUTLOOK

In summary, as a traditional semiconductor photocatalyst, TiO_2 has received extensive attention on its photocatalytic performance. However, the single TiO_2 always presents a limited photocatalytic efficiency, which is due to its rapid photo-induced carrier recombination, confined light-harvesting ability, and insufficient reduction ability. By constructing a TiO_2-based S-scheme heterojunction photocatalyst, it seems to be a very reasonable strategy to overcome the above shortcomings. In this case, this review gives a comprehensive summary of the classification of TiO_2-based S-scheme heterojunction photocatalysts, including metal oxides, metal chalcogenides, organic semiconductors, and other semiconductors. Besides, the potential applications of TiO_2-based S-scheme heterojunction photocatalysts in photocatalytic H_2 evolution, CO_2 reduction, H_2O_2 production, and pollutant degradation are described in detail. And, the characterization methods are also employed to explore the formation and photo-induced carrier transfer pathway of TiO_2-based S-scheme heterojunction photocatalysts.

Although the reported TiO_2-based S-scheme heterojunction

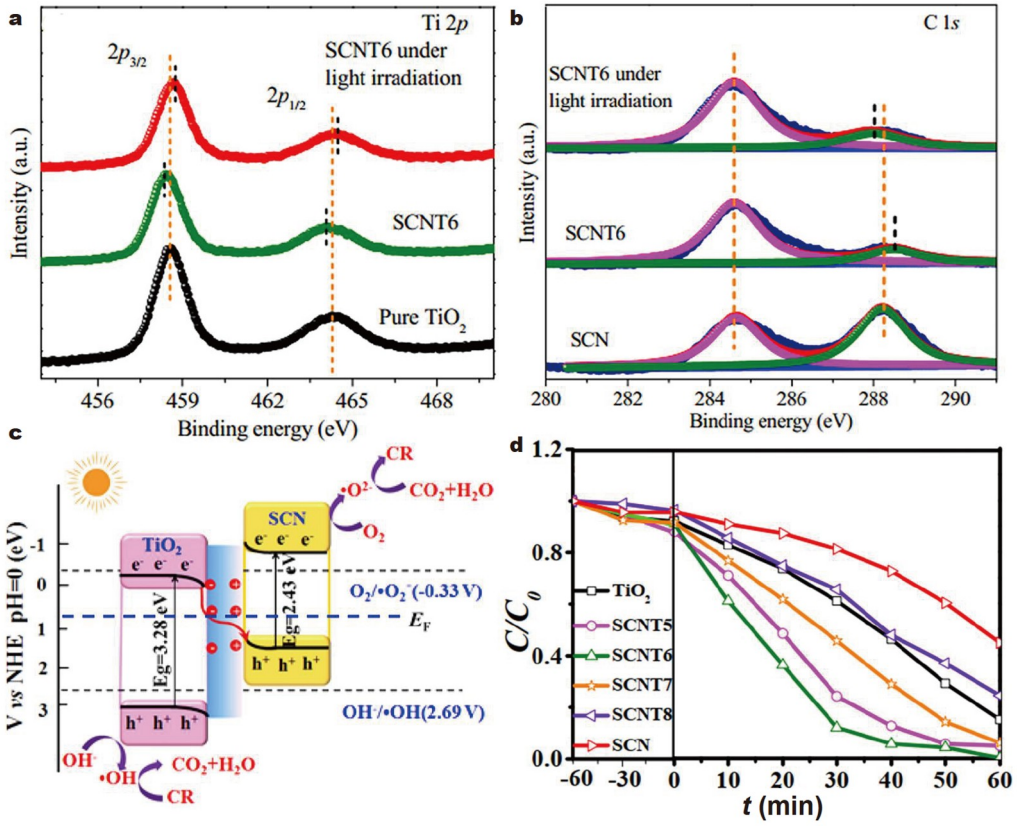

Figure 16 XPS spectra of (a) Ti 2p, (b) C 1s for TiO_2, SCN, and SCN/TiO_2 with and without light illumination, (c) photocatalytic mechanism of SCN/TiO_2, (d) photocatalytic Congo Red degradation efficiencies over different samples. Reprinted with permission from Ref. [147], Copyright 2021, Elsevier.

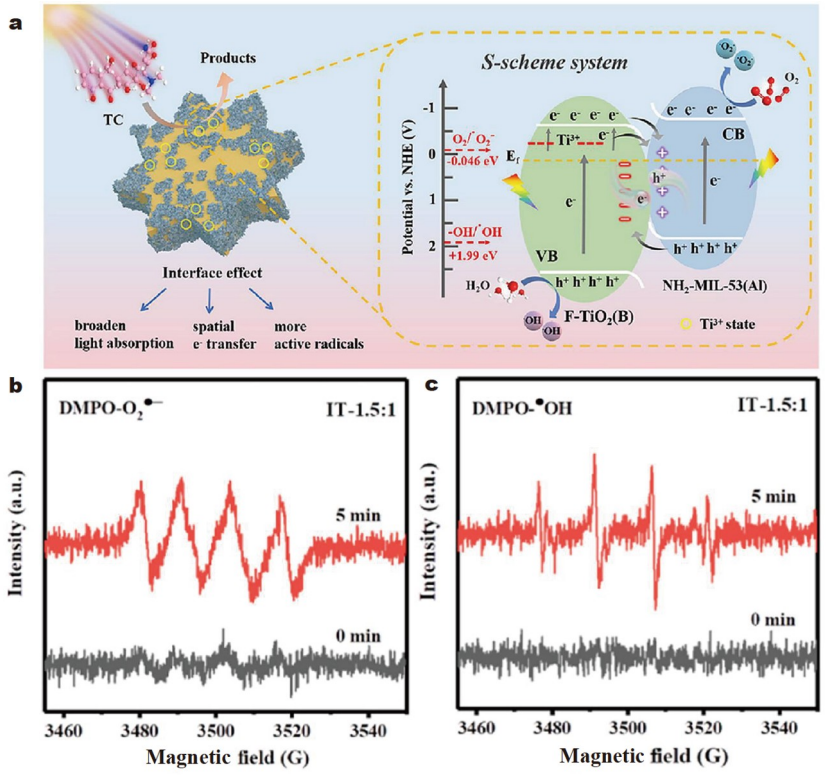

Figure 17 (a) Photocatalytic tetracycline degradation mechanism of NM(Al)/F-TiO_2(B). Reprinted with permission from Ref. [51], Copyright 2023, Elsevier. The electron spin resonance spectra of (b) DMPO-·O_2^- and (c) DMPO-·OH over In_2S_3/TiO_2(B). Reprinted with permission from Ref. [149], Copyright 2022, Elsevier.

photocatalysts can simultaneously obtain the broadened light absorption range, efficient photo-induced carrier separation and transfer, and strong redox capacity, thereby achieving the prominent photocatalytic efficiency. However, there are still some significant challenges in the future development of TiO_2-based S-scheme heterojunction photocatalysts that need to be further concerned and overcome in the following directions:

(1) Based on the formation mechanism of TiO_2-based S-scheme heterojunction photocatalyst, the internal electric field, energy band bending, as well as Coulombic attraction, can act as the driving forces to facilitate efficient photo-induced carrier separation and migration. However, it is rarely reported the relationship between them on photocatalytic performance. Thus, more attention should be paid to regulating the structure of heterojunctions in future research.

(2) Notably, TiO_2-based S-scheme heterojunction photocatalysts usually consist of two or more semiconductors. During a prolonged photocatalytic process, the S-scheme heterojunction often suffers from inadequate interfacial contact between semiconductors, thereby reducing the space charge region and photocatalytic performance. Thus, exploring the controllable synthesis methods are vital to strengthen interfacial interactions.

(3) By the *ex-* and *in situ* characterization methods and theoretical calculation, the formation mechanism of TiO_2-based S-scheme heterojunction photocatalysts has been confirmed. Due to the complexity of the photo-induced carrier transfer process, more characterization methods should be developed to reveal the photo-induced carrier transfer route, e.g., ultrafast transient absorption.

(4) Although the TiO_2-based S-scheme heterojunction photocatalysts obtain a broadly applications in the field of photocatalysis, there are few studies on photocatalytic N_2 fixation and CH_4 conversion. In fact, the TiO_2-based S-scheme heterojunction photocatalysts have potential applications in the above fields of photocatalysis. Thus, broadening the scope of application in future research is also essential.

(5) Currently, a major challenge faced by TiO_2-based S-scheme heterojunction photocatalysts is the insufficient utilization of solar energy to meet the practical requirements for commercial applications. For example, the maximum solar-to-hydrogen conversion efficiency for hydrogen production is far lower than the commercial standard (10%). Thus, it is necessary to improve the efficiency of solar energy utilization to meet its commercial applications.

Received 24 November 2023; accepted 4 January 2024; published online 23 January 2024

1 Liu DF, Sun B, Bai SJ, *et al.* Dual co-catalysts Ag/Ti_3C_2/TiO_2 hierarchical flower-like microspheres with enhanced photocatalytic H_2-production activity. Chin J Catal, 2023, 50: 273–283
2 Bie CB, Yu HG, Cheng B, *et al.* Design, fabrication, and mechanism of nitrogen-doped graphene-based photocatalyst. Adv Mater, 2021, 33: 2003521
3 Wei Z, Wang WC, Li WL, *et al.* Steering electron-hole migration pathways using oxygen vacancies in tungsten oxides to enhance their photocatalytic oxygen evolution performance. Angew Chem Int Ed, 2021, 60: 8236–8242
4 Jiang WB, Loh HY, Low BQL, *et al.* Role of oxygen vacancy in metal oxides for photocatalytic CO_2 reduction. Appl Catal B-Environ, 2023, 321: 122079
5 Zhu QH, Xu Q, Du MM, *et al.* Recent progress of metal sulfide photocatalysts for solar energy conversion. Adv Mater, 2022, 34: 2202929
6 Chakraborty J, Nath I, Verpoort F. A physicochemical introspection of porous organic polymer photocatalysts for wastewater treatment. Chem Soc Rev, 2022, 51: 1124–1138
7 Fujishima A, Honda K. Electrochemical photolysis of water at a semiconductor electrode. Nature, 1972, 238: 37–38
8 Sun B, Zhou GW, Zhang Y, *et al.* Photocatalytic properties of exposed crystal surface-controlled rutile TiO_2 nanorod assembled microspheres. Chem Eng J, 2015, 264: 125–133
9 Qu JS, Wang YS, Mu XL, *et al.* Determination of crystallographic orientation and exposed facets of titanium oxide nanocrystals. Adv Mater, 2022, 34: 2203320
10 Bayles A, Tian S, Zhou JY, *et al.* Al@TiO_2 core-shell nanoparticles for plasmonic photocatalysis. ACS Nano, 2022, 16: 5839–5850
11 Balakrishnan A, Appunni S, Chinthala M, *et al.* Biopolymer-supported TiO_2 as a sustainable photocatalyst for wastewater treatment: A review. Environ Chem Lett, 2022, 20: 3071–3098
12 Dong GM, Zhang YW, Wang YY, *et al.* Ti_3C_2 quantum dots modified 3D/2D TiO_2/g-C_3N_4 S-scheme heterostructures for highly efficient photocatalytic hydrogen evolution. ACS Appl Energy Mater, 2021, 4: 14342–14351
13 An XQ, Bian JY, Zhu K, *et al.* Facet-dependent activity of TiO_2/covalent organic framework S-scheme heterostructures for CO_2 photoreduction. Chem Eng J, 2022, 442: 135279
14 Li HP, Sun B, Gao TT, *et al.* Ti_3C_2 MXene co-catalyst assembled with mesoporous TiO_2 for boosting photocatalytic activity of methyl orange degradation and hydrogen production. Chin J Catal, 2022, 43: 461–471
15 Moradi M, Hasanvandian F, Isari AA, *et al.* CuO and ZnO co-anchored on g-C_3N_4 nanosheets as an affordable double Z-scheme nanocomposite for photocatalytic decontamination of amoxicillin. Appl Catal B-Environ, 2021, 285: 119838
16 You HJ, Liu R, Liang CC, *et al.* Gold nanoparticle doped hollow SnO_2 supersymmetric nanostructures for improved photocatalysis. J Mater Chem A, 2013, 1: 4097–4104
17 Sun B, Zhou GW, Gao TT, *et al.* NiO nanosheet/TiO_2 nanorod-constructed p-n heterostructures for improved photocatalytic activity. Appl Surf Sci, 2016, 364: 322–331
18 Rawool SA, Pai MR, Banerjee AM, *et al.* pn Heterojunctions in NiO: TiO_2 composites with type-II band alignment assisting sunlight driven photocatalytic H_2 generation. Appl Catal B-Environ, 2018, 221: 443–458
19 Zhu HL, Zhen C, Chen XT, *et al.* Patterning alternate TiO_2 and Cu_2O strips on a conductive substrate as film photocatalyst for Z-scheme photocatalytic water splitting. Sci Bull, 2022, 67: 2420–2427
20 Chen L, Song XL, Ren JT, *et al.* Precisely modifying Co_2P/black TiO_2 S-scheme heterojunction by *in situ* formed P and C dopants for enhanced photocatalytic H_2 production. Appl Catal B-Environ, 2022, 315: 121546
21 Alli YA, Oladoye PO, Matebese F, *et al.* Step-scheme photocatalysts: Promising hybrid nanomaterials for optimum conversion of CO_2. Nano Today, 2023, 53: 102006
22 Lu JN, Gu SN, Li HD, *et al.* Review on multi-dimensional assembled S-scheme heterojunction photocatalysts. J Mater Sci Tech, 2023, 160: 214–239
23 Xu QL, Zhang LY, Cheng B, *et al.* S-scheme heterojunction photocatalyst. Chem, 2020, 6: 1543–1559
24 Zhang LY, Zhang JJ, Yu HG, *et al.* Emerging S-scheme photocatalyst. Adv Mater, 2022, 34: 2107668
25 Cheng SW, Sun ZH, Lim KH, *et al.* Dual-defective two-dimensional/two-dimensional Z-scheme heterojunctions for CO_2 reduction. ACS Catal, 2023, 13: 7221–7229
26 Tada H, Mitsui T, Kiyonaga T, *et al.* All-solid-state Z-scheme in CdS-Au-TiO_2 three-component nanojunction system. Nat Mater, 2006, 5: 782–786
27 Xu QL, He RA, Li YJ. Problems and mistakes for electron transfer mechanism in Z-scheme photocatalytic system. Acta Phys-Chim Sin, 2023, 39: 2211009
28 Li YF, Xia ZL, Yang Q, *et al.* Review on g-C_3N_4-based S-scheme

heterojunction photocatalysts. J Mater Sci Tech, 2022, 125: 128–144
29 Fu JW, Xu QL, Low JX, *et al.* Ultrathin 2D/2D WO_3/g-C_3N_4 step-scheme H_2-production photocatalyst. Appl Catal B-Environ, 2019, 243: 556–565
30 Song MM, Song XH, Liu X, *et al.* Enhancing photocatalytic CO_2 reduction activity of $ZnIn_2S_4$/MOF-808 microsphere with S-scheme heterojunction by *in situ* synthesis method. Chin J Catal, 2023, 51: 180–192
31 Zhang YN, Xu MY, Zhou WQ, *et al.* Fabricated ZnO@$ZnIn_2S_4$ S-scheme heterojunction photocatalyst for enhanced electron-transfer and CO_2 reduction. J Colloid Interface Sci, 2023, 650: 1762–1772
32 Zhao H, Wang LR, Liu GH, *et al.* Hollow Rh-COF@COF S-scheme heterojunction for photocatalytic nicotinamide cofactor regeneration. ACS Catal, 2023, 13: 6619–6629
33 Lu JN, Wang YN, Li HD, *et al.* $Bi_2MoS_xO_{6-x}$/α-CoS crystalline/amorphous S-scheme heterojunction for visible light-driven targeted photo-decomposition of amoxicillin. Chem Eng J, 2023, 470: 144294
34 Jiang ZC, Cheng B, Zhang LY, *et al.* A review on ZnO-based S-scheme heterojunction photocatalysts. Chin J Catal, 2023, 52: 32–49
35 Wu XH, Chen GQ, Li LT, *et al.* $ZnIn_2S_4$-based S-scheme heterojunction photocatalyst. J Mater Sci Tech, 2023, 167: 184–204
36 Wang LX, Zhu BC, Zhang JJ, *et al.* S-scheme heterojunction photocatalysts for CO_2 reduction. Matter, 2022, 5: 4187–4211
37 Zhu JJ, Wageh S, Al-Ghamdi AA. Using the femtosecond technique to study charge transfer dynamics. Chin J Catal, 2023, 49: 5–7
38 Xu QL, Wageh S, Al-Ghamdi AA, *et al.* Design principle of S-scheme heterojunction photocatalyst. J Mater Sci Tech, 2022, 124: 171–173
39 Yang J, Xie TP, Mei YH, *et al.* High-efficiency V-mediated Bi_2MoO_6 photocatalyst for PMS activation: Modulation of energy band structure and enhancement of surface reaction. Appl Catal B-Environ, 2023, 339: 123149
40 Xie C, Xu L, Peng JH, *et al.* Halogenated Ti_3C_2 MXenes prepared by microwave molten salt for Hg^0 photo-oxidation. Adv Funct Mater, 2023, 33: 2213782
41 Guo Q, Zhou CY, Ma ZB, *et al.* Fundamentals of TiO_2 photocatalysis: Concepts, mechanisms, and challenges. Adv Mater, 2019, 31: 1901997
42 Liu LP, Liu XL, Chai YQ, *et al.* Surface modification of TiO_2 nanosheets with fullerene and zinc-phthalocyanine for enhanced photocatalytic reduction under solar-light irradiation. Sci China Mater, 2020, 63: 2251–2260
43 He F, Zhu BC, Cheng B, *et al.* 2D/2D/0D TiO_2/C_3N_4/Ti_3C_2 MXene composite S-scheme photocatalyst with enhanced CO_2 reduction activity. Appl Catal B-Environ, 2020, 272: 119006
44 He BW, Wang ZL, Xiao P, *et al.* Cooperative coupling of H_2O_2 production and organic synthesis over a floatable polystyrene-sphere-supported TiO_2/Bi_2O_3 S-scheme photocatalyst. Adv Mater, 2022, 34: 2203225
45 Wang YL, He WJ, Xiong J, *et al.* MIL-68 (In)-derived In_2O_3@TiO_2 S-scheme heterojunction with hierarchical hollow structure for selective photoconversion of CO_2 to hydrocarbon fuels. Fuel, 2023, 331: 125719
46 Yang Y, Cheng B, Yu JG, *et al.* TiO_2/In_2S_3 S-scheme photocatalyst with enhanced H_2O_2-production activity. Nano Res, 2023, 16: 4506–4514
47 Zhang ML, Miao H, Fan J, *et al.* Internal electric field-modulated S-scheme Ni_3Se_4/TiO_2 nanoparticle heterojunction for efficient photocatalytic H_2 evolution. ACS Appl Nano Mater, 2023, 6: 18284–18294
48 Wang LB, Cheng B, Zhang LY, *et al.* *In situ* irradiated XPS investigation on S-scheme TiO_2@$ZnIn_2S_4$ photocatalyst for efficient photocatalytic CO_2 reduction. Small, 2021, 17: 2103447
49 Bi F, Su YT, Zhang YL, *et al.* Vacancy-defect semiconductor quantum dots induced an S-scheme charge transfer pathway in 0D/2D structures under visible-light irradiation. Appl Catal B-Environ, 2022, 306: 121109
50 Yang Y, Liu JJ, Gu ML, *et al.* Bifunctional TiO_2/COF S-scheme photocatalyst with enhanced H_2O_2 production and furoic acid synthesis mechanism. Appl Catal B-Environ, 2023, 333: 122780
51 Zhu CZ, Yao HQ, Sun TY, *et al.* Ultrathin fluorine-doped TiO_2(B) nanosheets-anchored hierarchical cog wheel-shaped NH_2-MIL-53(Al) for boosting photocatalytic activity. Chem Eng J, 2023, 460: 141849
52 Dong ZL, Zhang ZJ, Jiang Y, *et al.* Embedding $CsPbBr_3$ perovskite quantum dots into mesoporous TiO_2 beads as an S-scheme heterojunction for CO_2 photoreduction. Chem Eng J, 2022, 433: 133762
53 Knezevic M, Hoang TH, Rashid N, *et al.* Recent development in metal halide perovskites synthesis to improve their charge-carrier mobility and photocatalytic efficiency. Sci China Mater, 2023, 66: 2545–2572
54 Li QQ, Zhao WL, Zhai ZC, *et al.* 2D/2D Bi_2MoO_6/g-C_3N_4 S-scheme heterojunction photocatalyst with enhanced visible-light activity by Au loading. J Mater Sci Tech, 2020, 56: 216–226
55 Wang C, Jiao H, Yang YB, *et al.* Dual-functional S-scheme Fe_3O_4/TiO_2/g-C_3N_4 double-heterostructure bridged by TiO_2 for collaborative removal of U(VI) and Sb(III). J Cleaner Production, 2023, 426: 139114
56 Liu HY, Sun F, Li XY, *et al.* g-C_3N_4/TiO_2/$ZnIn_2S_4$ graphene aerogel photocatalysts with double S-scheme heterostructure for improving photocatalytic multifunctional performances. Compos Part B-Eng, 2023, 259: 110746
57 Liu HX, Pan LK, Nie JL, *et al.* $Bi_{12}TiO_{20}$-TiO_2 S-scheme heterojunction for improved photocatalytic NO removal: Experimental and DFT insights. Separ Purif Tech, 2023, 314: 123575
58 Wang LX, Qiu JY, Wu N, *et al.* TiO_2/$CsPbBr_3$ S-scheme heterojunctions with highly improved CO_2 photoreduction activity through facet-induced Fermi level modulation. J Colloid Interface Sci, 2023, 629: 206–214
59 Shao XL, Li K, Li JP, *et al.* Investigating S-scheme charge transfer pathways in NiS@Ta_2O_5 hybrid nanofibers for photocatalytic CO_2 conversion. Chin J Catal, 2023, 51: 193–203
60 Zhou L, Li YF, Yang SJ, *et al.* Preparation of novel 0D/2D Ag_2WO_4/WO_3 step-scheme heterojunction with effective interfacial charges transfer for photocatalytic contaminants degradation and mechanism insight. Chem Eng J, 2021, 420: 130361
61 Wageh S, Al-Ghamdi AA, Xu QL. Core-shell Au@NiS_{1+x} cocatalyst for excellent TiO_2 photocatalytic H_2 production. Acta Physico Chim Sin, 2022, 0: 2202001–0
62 Xia PF, Cao SW, Zhu BC, *et al.* Designing a 0D/2D S-scheme heterojunction over polymeric carbon nitride for visible-light photocatalytic inactivation of bacteria. Angew Chem Int Ed, 2020, 59: 5218–5225
63 Cheng C, Zhang JJ, Zhu BC, *et al.* Verifying the charge-transfer mechanism in S-scheme heterojunctions using femtosecond transient absorption spectroscopy. Angew Chem Int Ed, 2023, 62: e202218688
64 Kim KH, Kim SJ, Choi WH, *et al.* Triphasic metal oxide photocatalyst for reaction site-specific production of hydrogen peroxide from oxygen reduction and water oxidation. Adv Energy Mater, 2022, 12: 2104052
65 Haque F, Daeneke T, Kalantar-zadeh K, *et al.* Two-dimensional transition metal oxide and chalcogenide-based photocatalysts. Nano-Micro Lett, 2018, 10: 1–27
66 Yuan Y, Guo RT, Hong LF, *et al.* A review of metal oxide-based Z-scheme heterojunction photocatalysts: Actualities and developments. Mater Today Energy, 2021, 21: 100829
67 Gao JS, Rao SS, Yu XH, *et al.* Dimensional-matched two dimensional/two dimensional TiO_2/Bi_2O_3 step-scheme heterojunction for boosted photocatalytic performance of sterilization and water splitting. J Colloid Interface Sci, 2022, 628: 166–178
68 He F, Meng AY, Cheng B, *et al.* Enhanced photocatalytic H_2-production activity of WO_3/TiO_2 step-scheme heterojunction by graphene modification. Chin J Catal, 2020, 41: 9–20
69 Liu Y, Huang DL, Cheng M, *et al.* Metal sulfide/MOF-based composites as visible-light-driven photocatalysts for enhanced hydrogen production from water splitting. Coord Chem Rev, 2020, 409: 213220
70 Yin J, Jin J, Lin HH, *et al.* Optimized metal chalcogenides for boosting water splitting. Adv Sci, 2020, 7: 1903070
71 Chen SS, Ma GJ, Wang Q, *et al.* Metal selenide photocatalysts for visible-light-driven *Z*-scheme pure water splitting. J Mater Chem A, 2019, 7: 7415–7422
72 Wang F, Huang FX, Yu FB, *et al.* Metal-sulfide photocatalysts for solar-fuel generation across the solar spectrum. Cell Rep Phys Sci, 2023, 4: 101450
73 Zhu SC, Xiao FX. Transition metal chalcogenides quantum dots: Emerging building blocks toward solar-to-hydrogen conversion. ACS

Catal, 2023, 13: 7269–7309
74 Wang YC, Ren BY, Ou JZ, *et al.* Engineering two-dimensional metal oxides and chalcogenides for enhanced electro- and photocatalysis. Sci Bull, 2021, 66: 1228–1252
75 Wang JJ, Lin S, Tian N, *et al.* Nanostructured metal sulfides: Classification, modification strategy, and solar-driven CO_2 reduction application. Adv Funct Mater, 2021, 31: 2008008
76 Park H, Kim S, Kim T, *et al.* CoS@TiO_2 S-scheme heterojunction photocatalyst for hydrogen production from photoinduced water splitting. J Cleaner Prod, 2021, 319: 128819
77 Wang QY, Zhu SX, Zhao SZ, *et al.* Construction of Bi-assisted modified CdS/TiO_2 nanotube arrays with ternary S-scheme heterojunction for photocatalytic wastewater treatment and hydrogen production. Fuel, 2022, 322: 124163
78 Wang QP, Wang GH, Wang J, *et al. In situ* hydrothermal synthesis of ZnS/TiO_2 nanofibers S-scheme heterojunction for enhanced photocatalytic H_2 evolution. Adv Sustain Syst, 2023, 7: 2200027
79 Zhang XD, Zeng YX, Shi WY, *et al.* S-scheme heterojunction of core-shell biphase (1T-2H)-$MoSe_2$/TiO_2 nanorod arrays for enhanced photoelectrocatalytic production of hydrogen peroxide. Chem Eng J, 2022, 429: 131312
80 He BW, Xiao P, Wan SJ, *et al.* Rapid charge transfer endowed by interfacial Ni-O bonding in S-scheme heterojunction for efficient photocatalytic H_2 and imine production. Angew Chem Int Ed, 2023, 62: e202313172
81 Khamrai J, Das S, Savateev A, *et al.* Mizoroki-Heck type reactions and synthesis of 1, 4-dicarbonyl compounds by heterogeneous organic semiconductor photocatalysis. Green Chem, 2021, 23: 2017–2024
82 Li YR, Wang ZW, Xia T, *et al.* Implementing metal-to-ligand charge transfer in organic semiconductor for improved visible-near-infrared photocatalysis. Adv Mater, 2016, 28: 6959–6965
83 Wang L, Huang W, Li R, *et al.* Structural design principle of small-molecule organic semiconductors for metal-free, visible-light-promoted photocatalysis. Angew Chem Int Ed, 2016, 55: 9783–9787
84 Chen YZ, Yan CX, Dong JQ, *et al.* Structure/property control in photocatalytic organic semiconductor nanocrystals. Adv Funct Mater, 2021, 31: 2104099
85 Liu SS, Wang MF, He YZ, *et al.* Covalent organic frameworks towards photocatalytic applications: Design principles, achievements, and opportunities. Coord Chem Rev, 2023, 475: 214882
86 Wang LB, Fei XG, Zhang LY, *et al.* Solar fuel generation over nature-inspired recyclable TiO_2/g-C_3N_4 S-scheme hierarchical thin-film photocatalyst. J Mater Sci Tech, 2022, 112: 1–10
87 Meng AY, Cheng B, Tan HY, *et al.* TiO_2/polydopamine S-scheme heterojunction photocatalyst with enhanced CO_2-reduction selectivity. Appl Catal B-Environ, 2021, 289: 120039
88 Zhang BK, Wang DB, Jiao SJ, *et al.* TiO_{2-X} mesoporous nanospheres/BiOI nanosheets S-scheme heterostructure for high efficiency, stable and unbiased photocatalytic hydrogen production. Chem Eng J, 2022, 446: 137138
89 Zhao ZW, Ling Q, Li ZL, *et al.* S-scheme $BaTiO_3$/TiO_2 heterojunctions: Piezophotocatalytic degradation of norfloxacin. Separation Purification Tech, 2023, 308: 122928
90 Wang KX, Luo ZG, Xiao B, *et al.* S-scheme Cu_3P/TiO_2 heterojunction for outstanding photocatalytic water splitting. J Colloid Interface Sci, 2023, 652: 1908–1916
91 Zhao LN, Bian J, Zhang XF, *et al.* Construction of ultrathin S-scheme heterojunctions of single Ni atom immobilized Ti-MOF and $BiVO_4$ for CO_2 photoconversion of nearly 100% to CO by pure water. Adv Mater, 2022, 34: 2205303
92 Liu BW, Cai JJ, Zhang JJ, *et al.* Simultaneous benzyl alcohol oxidation and H_2 generation over MOF/CdS S-scheme photocatalysts and mechanism study. Chin J Catal, 2023, 51: 204–215
93 Zhang YF, Liu HX, Gao FX, *et al.* Application of MOFs and COFs for photocatalysis in CO_2 reduction, H_2 generation, and environmental treatment. EnergyChem, 2022, 4: 100078
94 Su B, Huang HW, Ding ZX, *et al.* S-scheme $CoTiO_3$/$Cd_{9.51}Zn_{0.49}S_{10}$ heterostructures for visible-light driven photocatalytic CO_2 reduction. J Mater Sci Tech, 2022, 124: 164–170
95 Hao L, Huang HW, Zhang YH, *et al.* Oxygen vacant semiconductor photocatalysts. Adv Funct Mater, 2021, 31: 2100919
96 Chen ZY, Huang NY, Xu Q. Metal halide perovskite materials in photocatalysis: Design strategies and applications. Coord Chem Rev, 2023, 481: 215031
97 Weng CC, Ren JT, Yuan ZY. Transition metal phosphide-based materials for efficient electrochemical hydrogen evolution: A critical review. ChemSusChem, 2020, 13: 3357–3375
98 Jaryal R, Kumar R, Khullar S. Mixed metal-metal organic frameworks (MM-MOFs) and their use as efficient photocatalysts for hydrogen evolution from water splitting reactions. Coord Chem Rev, 2022, 464: 214542
99 Lei ZN, Cao XF, Fan J, *et al.* Efficient photocatalytic H_2 generation over $In_{2.77}S_4$/NiS_2/g-C_3N_4 S-scheme heterojunction using NiS_2 as electron-bridge. Chem Eng J, 2023, 457: 141249
100 Wageh S, Al-Ghamdi AA, Al-Hartomy OA, *et al.* CdS/polymer S-scheme H_2-production photocatalyst and its *in situ* irradiated electron transfer mechanism. Chin J Catal, 2022, 43: 586–588
101 Shen RC, Ren DD, Ding YN, *et al.* Nanostructured CdS for efficient photocatalytic H_2 evolution: A review. Sci China Mater, 2020, 63: 2153–2188
102 Wu XH, Chen GQ, Wang J, *et al.* Review on S-scheme heterojunctions for photocatalytic hydrogen evolution. Acta Physico Chim Sin, 2023, 0: 2212016
103 Wan SJ, Xu JS, Cao SW, *et al.* Promoting intramolecular charge transfer of graphitic carbon nitride by donor-acceptor modulation for visible-light photocatalytic H_2 evolution. Interdiscipl Mater, 2022, 1: 294–308
104 Nishioka S, Osterloh FE, Wang XC, *et al.* Photocatalytic water splitting. Nat Rev Methods Primers, 2023, 3: 42
105 Bie CB, Wang LX, Yu JG. Challenges for photocatalytic overall water splitting. Chem, 2022, 8: 1567–1574
106 Wang LX, Yu JG. Photocatalytic phosphine-mediated water activation generates hydrogen atom radicals for transfer hydrogenation of closed-shell π systems. Sci China Mater, 2023, 66: 4133–4134
107 Mehta A, Mishra A, Basu S, *et al.* Band gap tuning and surface modification of carbon dots for sustainable environmental remediation and photocatalytic hydrogen production: A review. J Environ Manage, 2019, 250: 109486
108 Li JM, Wu CC, Li J, *et al.* 1D/2D TiO_2/$ZnIn_2S_4$ S-scheme heterojunction photocatalyst for efficient hydrogen evolution. Chin J Catal, 2022, 43: 339–349
109 Huang WQ, Xue WH, Hu XY, *et al.* A S-scheme heterojunction of Co_9S_8 decorated TiO_2 for enhanced photocatalytic H_2 evolution. J Alloys Compd, 2023, 930: 167368
110 Yang SY, Wang KL, Chen Q, *et al.* Enhanced photocatalytic hydrogen production of S-scheme TiO_2/g-C_3N_4 heterojunction loaded with single-atom Ni. J Mater Sci Tech, 2024, 175: 104–114
111 Zhang YP, Han W, Yang Y, *et al.* S-scheme heterojunction of black TiO_2 and covalent-organic framework for enhanced photocatalytic hydrogen evolution. Chem Eng J, 2022, 446: 137213
112 Shaheer ARM, Vinesh V, Lakhera SK, *et al.* Reduced graphene oxide as a solid-state mediator in TiO_2/$In_{0.5}WO_3$ S-scheme photocatalyst for hydrogen production. Sol Energy, 2021, 213: 260–270
113 Bai X, Fu ZY, Ma XY, *et al.* Hydrophilic regulated photocatalytic converting phenol selectively over S-scheme $CuWO_4$/TiO_2. J Cleaner Production, 2022, 369: 133099
114 Liu XJ, Chen TQ, Xue YH, *et al.* Nanoarchitectonics of MXene/semiconductor heterojunctions toward artificial photosynthesis *via* photocatalytic CO_2 reduction. Coord Chem Rev, 2022, 459: 214440
115 Xia Y, Cheng B, Fan JJ, *et al.* Near-infrared absorbing 2D/3D $ZnIn_2S_4$/N-doped graphene photocatalyst for highly efficient CO_2 capture and photocatalytic reduction. Sci China Mater, 2020, 63: 552–565
116 Li DD, Kassymova M, Cai XC, *et al.* Photocatalytic CO_2 reduction over metal-organic framework-based materials. Coord Chem Rev, 2020, 412: 213262
117 Albero J, Peng Y, García H. Photocatalytic CO_2 reduction to C2+ Products. ACS Catal, 2020, 10: 5734–5749
118 Ouyang TW, Guo JQ, Shen HC, *et al.* The Z-scheme transfer of

photogenerated electrons for CO_2 photocatalytic reduction over g-ZnO/2H-MoS_2 heterostructure. Nanoscale, 2021, 13: 18192–18200
119 Su B, Zheng M, Lin W, *et al.* S-scheme Co_9S_8@$Cd_{0.8}Zn_{0.2}$S-DETA hierarchical nanocages bearing organic CO_2 activators for photocatalytic syngas production. Adv Energy Mater, 2023, 13: 2203290
120 Chen GJ, Zhou ZR, Li BF, *et al.* S-scheme heterojunction of crystalline carbon nitride nanosheets and ultrafine WO_3 nanoparticles for photocatalytic CO_2 reduction. J Environ Sci, 2023, doi: 10.1016/j.jes.2023.05.028
121 Wang K, Cheng Q, Hou WD, *et al.* Unlocking the charge-migration mechanism in S-scheme junction for photoreduction of diluted CO_2 with high selectivity. Adv Funct Mater, 2023, doi: 10.1002/adfm.202309603
122 Fang SY, Rahaman M, Bharti J, *et al.* Photocatalytic CO_2 reduction. Nat Rev Methods Primers, 2023, 3: 61
123 Xie F, Bie CB, Sun J, *et al.* A DFT study on Pt single atom loaded COF for efficient photocatalytic CO_2 reduction. J Mater Sci Tech, 2024, 170: 87–94
124 Hasija V, Kumar A, Sudhaik A, *et al.* Step-scheme heterojunction photocatalysts for solar energy, water splitting, CO_2 conversion, and bacterial inactivation: A review. Environ Chem Lett, 2021, 19: 2941–2966
125 Ren GM, Wei ZX, Li ZZ, *et al.* Fabrication of S-scheme hollow TiO_2@Bi_2MoO_6 composite for efficiently photocatalytic CO_2 reduction. Mater Today Chem, 2023, 27: 101260
126 Hezam A, Alkanad K, Bajiri MA, *et al.* 2D/1D MoS_2/TiO_2 heterostructure photocatalyst with a switchable CO_2 reduction product. Small Methods, 2023, 7: 2201103
127 Liang SM, Chen YJ, Han W, *et al.* Hierarchical S-scheme titanium dioxide@cobalt-nickel based metal-organic framework nanotube photocatalyst for selective carbon dioxide photoreduction to methane. J Colloid Interface Sci, 2023, 630: 11–22
128 Kim J, Kim JH, Oh C, *et al.* Electro-assisted methane oxidation to formic acid *via in situ* cathodically generated H_2O_2 under ambient conditions. Nat Commun, 2023, 14: 4704
129 Wu Y, Yang Y, Gu ML, *et al.* 1D/0D heterostructured $ZnIn_2S_4$@ZnO S-scheme photocatalysts for improved H_2O_2 preparation. Chin J Catal, 2023, 53: 123–133
130 Zhu BC, Liu JJ, Sun J, *et al.* CdS decorated resorcinol-formaldehyde spheres as an inorganic/organic S-scheme photocatalyst for enhanced H_2O_2 production. J Mater Sci Tech, 2023, 162: 90–98
131 Jiang ZC, Long Q, Cheng B, *et al.* 3D ordered macroporous sulfur-doped g-C_3N_4/TiO_2 S-scheme photocatalysts for efficient H_2O_2 production in pure water. J Mater Sci Tech, 2023, 162: 1–10
132 He RG, Xu DF, Li X. Floatable S-scheme photocatalyst for H_2O_2 production and organic synthesis. J Mater Sci Tech, 2023, 138: 256–258
133 Zhao Y, Li XK, Fan X, *et al.* Small-molecule catalyzed H_2O_2 production *via* a phase-transfer photocatalytic process. Appl Catal B-Environ, 2022, 314: 121499
134 Xia CH, Yuan L, Song H, *et al.* Spatial specific Janus S-scheme photocatalyst with enhanced H_2O_2 production performance. Small, 2023, 19: 2300292
135 Zhang KY, Li YF, Yuan SD, *et al.* Review of S-scheme heterojunction photocatalyst for H_2O_2 production. Acta Physico Chim Sin, 2023, 39: 2212010
136 Che HN, Gao X, Chen J, *et al.* Iodide-induced fragmentation of polymerized hydrophilic carbon nitride for high-performance quasi-homogeneous photocatalytic H_2O_2 production. Angew Chem Int Ed, 2021, 60: 25546–25550
137 Zhang HZ, Liu JJ, Zhang Y, *et al.* BiOBr/COF S-scheme photocatalyst for H_2O_2 production *via* concerted two-electron pathway. J Mater Sci Tech, 2023, 166: 241–249
138 Wang K, Li JP, Liu XF, *et al.* Sacrificial-agent-free artificial photosynthesis of hydrogen peroxide over step-scheme WO_3/NiS hybrid nanofibers. Appl Catal B-Environ, 2024, 342: 123349
139 Sun B, Tao FR, Huang ZX, *et al.* Ti_3C_2 MXene-bridged Ag/Ag_3PO_4 hybrids toward enhanced visible-light-driven photocatalytic activity. Appl Surf Sci, 2021, 535: 147354
140 Wu YW, Zhong LL, Yuan JL, *et al.* Photocatalytic optical fibers for degradation of organic pollutants in wastewater: A review. Environ Chem Lett, 2021, 19: 1335–1346
141 Sun B, Dong XS, Li HP, *et al.* Surface charge engineering for two-dimensional Ti_2CT_x MXene for highly efficient and selective removal of cationic dye from aqueous solution. Separat Purif Tech, 2021, 272: 118964
142 Zada A, Khan M, Khan MA, *et al.* Review on the hazardous applications and photodegradation mechanisms of chlorophenols over different photocatalysts. Environ Res, 2021, 195: 110742
143 Rasouli K, Rasouli J, Mohtaram MS, *et al.* Biomass-derived activated carbon nanocomposites for cleaner production: A review on aspects of photocatalytic pollutant degradation. J Cleaner Prod, 2023, 419: 138181
144 Wang HH, Duan YH, Fei GQ, *et al.* Design, synthesis and modification of 2D nanomaterials-based photocatalysts for pollutant degradation and photodegradation experiments from lab-scale to grand-scale. Chem Eng J, 2023, 477: 147219
145 Li CG, Tian Q, Zhang YL, *et al.* Sequential combination of photocatalysis and microalgae technology for promoting the degradation and detoxification of typical antibiotics. Water Res, 2022, 210: 117985
146 Wang ZZ, Li Y, Cheng Q, *et al.* Sb-based photocatalysts for degradation of organic pollutants: A review. J Cleaner Prod, 2022, 367: 133060
147 Wang J, Wang GH, Cheng B, *et al.* Sulfur-doped g-C_3N_4/TiO_2 S-scheme heterojunction photocatalyst for Congo Red photodegradation. Chin J Catal, 2021, 42: 56–68
148 He RG, Liu HJ, Liu HM, *et al.* S-scheme photocatalyst Bi_2O_3/TiO_2 nanofiber with improved photocatalytic performance. J Mater Sci Tech, 2020, 52: 145–151
149 Zhu CZ, Yao HQ, Le SK, *et al.* S-scheme photocatalysis induced by ultrathin TiO_2(B) nanosheets-anchored hierarchical In_2S_3 spheres for boosted photocatalytic activity. Compos Part B-Eng, 2022, 242: 110082
150 Li Z, Ai W, Zhang YH, *et al.* Magnetic carbon nanotube modified S-scheme TiO_{2-x}/g-C_3N_4/CNFe heterojunction coupled with peroxymonosulfate for effective visible-light-driven photodegradation *via* enhanced interfacial charge separation. Separat Purif Tech, 2023, 308: 122897
151 Tang RD, Gong DX, Deng YC, *et al.* π-π Stacked step-scheme PDI/g-C_3N_4/TiO_2@Ti_3C_2 photocatalyst with enhanced visible photocatalytic degradation towards atrazine *via* peroxymonosulfate activation. Chem Eng J, 2022, 427: 131809
152 Zhu YK, Zhuang Y, Wang LL, *et al.* Constructing 0D/1D Ag_3PO_4/TiO_2 S-scheme heterojunction for efficient photodegradation and oxygen evolution. Chin J Catal, 2022, 43: 2558–2568

Acknowledgements This work was supported by the National Natural Science Foundation of China (52202102 and 51972180), the Natural Science Foundation of Shandong Province (ZR2019BB030 and ZR2020ME082), the Science and Technology Support Plan for Youth Innovation of Colleges and Universities of Shandong Province (2021KJ056), the Science Fund of Shandong Laboratory of Advanced Materials and Green Manufacturing at Yantai (AMGM2023F13 and AMGM2021F05), the Undergraduate Training Program on Innovation and Entrepreneurship of Shandong Province (S202210431016) and the Science, Education and Industry Integration of Basic Research Projects of Qilu University of Technology (2023PY022).

Author contributions Sun B and Zhou G proposed the theme and outline of the manuscript. Zhang B and Liu F collected the relevant information about the manuscript. Zhang B wrote the first draft. Sun B, Gao T, and Zhou G revised the manuscript. All authors discussed, commented, and supervised on the manuscript.

Conflict of interest The authors declare no conflict of interest.

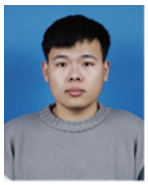

Baolong Zhang is pursuing a Master degree at the School of Chemistry and Chemical Engineering, Qilu University of Technology. His research focuses on the controllable preparation of S-scheme heterojunction photocatalysts and their applications to photocatalytic hydrogen evolution.

Bin Sun received his PhD degree in 2018 from the State Key Laboratory of Crystal Materials, Shandong University. Now he is an associate professor at the School of Chemistry and Chemical Engineering, Qilu University of Technology. His research interest is mainly focused on the controlled synthesis of low-dimensional nanostructured materials for energy conversion and environmental remediation applications.

Guowei Zhou received his BS, MS, and PhD degrees at Shandong University (1986, 1989 and 2001). He carried out postdoctoral research at Pukyong National University (2012–2013) and the Hong Kong University of Science and Technology (2015–2016). He is currently a Professor at Qilu University of Technology. His research interests include the controlled synthesis and hierarchical assembly mesostructure functional materials with specific morphology and the application of ordered mesoporous materials for catalysis, and energy conversion and storage.

用于能源转化和环境修复的TiO_2基梯型异质结光催化剂

张宝龙, 孙彬*, 刘方璇, 高婷婷, 周国伟*

摘要 太阳能驱动的半导体光催化技术被认为是缓解能源短缺和环境污染的潜在策略. 因此, 探索高效的光催化剂是推动光催化技术发展和实际应用的关键. 作为一种典型的半导体光催化剂, TiO_2因其化学稳定、环境友好、成本低廉等特性而备受关注. 然而, TiO_2光生载流子的快速复合、光吸收范围窄以及还原能力不足等缺点严重阻碍了其光催化性能. 通过将TiO_2与其他半导体复合以构建梯型异质结可以有效的解决上述问题. 在此光催化体系中, 梯型异质结不仅可以整合各组分的优点, 实现光生载流子的有效分离和光捕获能力的增强, 而且还能保留最强的氧化还原能力. 基于此, 本文综述了利用构建梯型异质结来提高TiO_2光催化性能的最新研究进展, 着重介绍了TiO_2基梯型异质结光催化剂的分类, 主要包括金属氧化物、金属硫属化物、有机半导体和其他类型半导体. 在此基础上, 本文还总结了TiO_2基梯型异质结光催化剂在析氢、CO_2还原、H_2O_2生成和污染物降解等领域中的应用. 同时, 为了更好地理解光生载流子的转移途径, 本文还简要介绍了梯型异质结的一些表征方法. 最后, 对TiO_2基梯型异质结光催化剂所面临的问题和未来的发展方向进行了展望. 综上, 本文旨在为构建用于能源转换和环境修复的高效TiO_2基梯型异质结光催化剂提供参考.